Obtaining structural data of the pore-forming region of the *Shaker* potassium channel using the scorpion toxin Agitoxin2

Tesis
entregada a la
Universidad de Chile
en cumplimiento parcial de los requisitos
para optar al grado de
Doctor en Ciencias con mención en Biología

Facultad de Ciencias

por

Patricia Hidalgo Jimenez
Mayo, 1995

Director de tesis: Dr. Roderick Mackinnon
Dr. Pedro Labarca

FACULTAD DE CIENCIAS
UNIVERSIDAD DE CHILE

INFORME DE APROBACION
TESIS DE DOCTORADO

Se informa a la Comisión de Postgrado de la Facultad de Ciencias que la Tesis de Doctorado presentada por el candidato.

Patricia Hidalgo

Ha sido aprobada por la Comisión de Evaluación de la Tesis como requisito de tesis para optar al grado de Doctor en Ciencias con mención en Biología, en el Examen de Defensa de Tesis rendido el día 21 de abril de 1995.

Director de Tesis

Dr. Roderick MacKinnon

Dr. PEDRO LABARCA

Comisión de Evaluación de la Tesis

Dr. OSVALDO ALVAREZ

Dr. Ramón Latorre

Dr. Catherine Connelly M.

Dr. NIBALDO INESTROSA C

Dr. Francisco Sepúlveda

.....a mis padres que sucede que son mis mejores amigos

AGRADECIMIENTOS

Es cierto
si estas solo
llegaras facilmente
al desparpajo contigo mismo...

Mario Benedetti

A muchos debo la alegría, la pasión, la energía y el esfuerzo vertidos en esta tesis. En su transcurso aprendí a ver el mundo a través de los ojos de distintas culturas.

Agradezco infinitamente el amor de mis padres que ha sido siempre mi voluntad para emprender.

Agradezco a mis profesores, Pedro Labarca por transmitirme la pasión en cada aventura científica, por pensar en mi futuro cuando yo volaba en el presente y por empujarme a partir (espero no intentabas deshacerte de mi!!). Ramon Latorre, por la confianza, la alegría de vivir y el buen consejo. Osvaldo Alvarez por el claro pensamiento y la digna consecuencia sobretodo y aún mas en esos tiempos de escasez. Y en el norte y en otra lengua agradezco a Rod MacKinnon por la ciencia y la no ciencia, por la paciencia y también por la impaciencia, por la maravilla del pensamiento humano, por enseñarme pausadamente las reglas

de aquel mundo tan fuerte. Por la confianza y la promesa del canto a viva voz (aunque no haya sido necesario).

Agradezco a mis hermanos y amigos, Bernardo Morales, mi yunta y compinche. Felipe Díaz, el de siempre, el de toda la vida. Gonzalo Ugarte, la viva alegría, Nataniel Malebran, el buen amigo. A todos ellos por un tiempo hermoso, por la solidaridad y por la risa a carcajadas.

Agradezco a Ricardo Delgado por enseñarme pacientemente cuando apenitas si entendía. A Ximena Cecchi Y Cecilia Vergara por las sonrisas cómplices. A Juan Bacigalupo y Daniel Wolff por el tiempo otorgado a cada pregunta. A Juan Espinoza por la resistencia, a mi incapacidad electrónica. A Anita y Luisa y Marcelo, siempre atentos.

Y nuevamente mirando al norte, agradezco a Lise Heginbotham por el esfuerzo de entender desde el mas comienzo mis guturaciones en inglés y así responder mi ataque de preguntas. A Tanya Abramson por enseñarme cada truco, cada detalle de lo nuevo y por saber lo que estaba pensando. A Laura Escobar, la palabra amiga. A Mike Root porque pese al volumen de la radio igual escuchó mis gritos de auxilio (y de apaga la radio!!!). A Adrian Gross, el cariño dulce y la sonrisa reconfortante que alegra el corazón. A Sanjey, la buena voluntad. A Chul-Seung Park por la sonrisas y gestos gentiles cotidianos (y por los primers!!!). A Rama, por el humor compartido.

Agradezco a Ken Swartz a ese gringo buen amigo, por la comprensión y el buen humor; por las palabras de apoyo y a

estas alturas también por las palabrotas!!. Agradezco desde muy dentro a mi gran amigo ZHE LU así con mayúsculas, a ZHE quien tuvo siempre, a cada instante, la palabra certera, justa y solidaria.

También agradezco a Felipe Martinez por ser el gran soporte en los primeros pasos , que son los tambaleantes. Y a Juan Carlos Cerda, por el cariño inmenso.

A Verónica Cambiazo por la hospitalidad, tesoro del recién llegado. A Tere Silva y Miguel Allende por su constante preocupación del bienestar de mi alma y por suerte también de mi salud. A mi familia postiza, compatriotas que estan tambien en el norte, David Naranjo, la voz familiar necesaria al comenzar, Alfredo Kirwood, Ricardo Araneda, a todos ellos por las costumbres compartidas que nos fortalecen. A Adrián Palacios, el apoyo tranquilo, indispensable e intenso, porque mi corazón estaba contento y ma que mal, a corazón contento mejores son la tesis!!!.

Agradezco con la profunda alegría de sentirse tan afortunada, quien diría que al final del viaje, en el otro extremo estaba una hermana, Julie Nardone, quien tradujo tan fielmente al inglés la palabra amistad, porque conte con ella siempre y puchas que conte!!!!

Y gracias a muchos anónimos que no son anónimos pero que tal vez deje en el olvido, es que como siempre también estoy atrasada con esta tesis...

Agradezco a la Comision Nacional de Investigación Científica y Tecnológica (CONICYT) y al Centro de Estudios Científicos de Santiago (CECS) por el financiamiento

otorgado para realizar mis estudios de doctorado.

Prefacio

Esta Tesis ha sido escrita en inglés. El motivo principal es que fue realizada en el Departamento de Neurobiología de la Escuela de Medicina de Harvard bajo la guía del Dr. Roderick MacKinnon, quién no habla español. Escribir mi Tesis en inglés me dió la posibilidad de gozar del beneficioso "feed-back", a través de la discusión, que se tradujo finalmente en un aporte positivo a mi Tesis. Esta Tesis en inglés también es en gratitud a un excelente guía como lo fue el Dr. MacKinnon quién podrá así disfrutar de la lectura de ésta.

El trabajo realizado en esta Tesis está descrito en cuatro capítulos los cuales siguen el curso temporal de mi labor experimental, y cuyo contenido forma parte de cuatro publicaciones como sigue:

Capítulo 2. Purification and characterization of three inhibitors of voltage-dependent K^+ channels from Leiurus Quinquestriatus var. hebraeus venom. Garcia, M.L., Garcia-Calvo, M., Hidalgo, P., Lee, A., and MacKinnon, R. (1994). *Biochemistry 33*, 6834-6839.

Capítulo 3. Solution structure of the potassium channel inhibitor Agitoxin 2: Calipers for probing channel geometry. Krezel, A., Khasibhatla, C., Hidalgo, P., MacKinnon, R., and Wagner, G. (1995). *Prot. Sci. In Press,*

Capítulo 4. Revealing the architecture of a K^+ channel pore through mutant cycles with a peptide inhibitor. Hidalgo, P. and MacKinnon, R. (1995). *Science 268,* 307-310.

Capítulo 5. Manuscript in preparation

TABLE OF CONTENTS

LIST OF FIGURES

Chapter 4.

Chapter 5.

General Discussion

LIST OF TABLES

ABBREVIATIONS

AgTx	agitoxin
ChTx	charybdotoxin
HPLC	high performance liquid chromatography
IbTx	iberiotoxin
IPTG	isopropyl β-D-thiogalactoside
Ktx	kaliotoxin
Lq2	*Leiurus quinquestriatus* toxin
MgTx	margatoxin
NMR	nuclear magnetic resonance
NxTx	noxiustoxin
PCR	polymerase chain reaction
TEA	tetraethylammonium ion

ABBREVIATION OF SUBSTITUTED PROTEINS

Substituted proteins are named with a shorthand designation consisting of *(wild type amino acid) (position number) (substituted amino acid)*. For example, if position 24 in the wild type protein is arginine, and it has been changed to glutamine by mutation, then the resulting mutant protein is designated R24Q. Amino acid residues are referred to by the appropriate three-letter code followed by the position number. The one- and three-letter codes for amino acids are given below.

A	ala	alanine
C	cys	cysteine
D	asp	aspartate
E	glu	glutamate
F	phe	phenylalanine
G	gly	glycine
H	his	histidine
I	ile	isoleucine
K	lys	lysine
L	leu	leucine
M	met	methionine
N	asn	asparagine
P	pro	proline
Q	gln	glutamine
R	arg	arginine
S	ser	serine
T	thr	threonine
V	val	valine
W	trp	tryptophan
Y	tyr	tyrosine
Z	pyr	pyroglutamate

RESUMEN

Los canales de K^+ constituyen el grupo más diverso dentro de la familia de los canales iónicos. Ellos se activan en respuesta a cambios en el potencial de membrana, a segundos mensajeros como AMPc o Ca^{2+} y vía proteína G. Pese a la gran diversidad en sus mecanismos de activación, todos ellos exhiben una alta selectividad por iones K^+. Esto significa que son capaces de excluir iones Na^+ aún cuando estos últimos poseen un radio atómico menor.

Para entender las bases moleculares de la selectividad iónica en canales de K^+ se requiere tanto de datos funcionales como de información estructural. Hasta ahora ningún canal de K^+ ha sido purificado en grandes cantidades. En consecuencia carecemos de cualquier información estructural obtenida mediante el uso de técnicas directas de determinación de estructura de proteínas.

Mi trabajo de tesis consistió en el estudio de la interacción entre un inhibidor peptídico recientemente aislado del veneno de scorpion, Agitoxina2 (AgTx2), y el canal de K^+ activado por voltaje denominado *Shaker*. El objetivo fundamental es usar AgTx2 como una sonda para obtener información acerca de la estructura del sitio de unión de este inhibidor en el canal. El primer paso hacia este objetivo fue la síntesis de AgTx2 usando técnicas de DNA recombinante y la caracterización funcional de AgTx2. El segundo paso, crucial para el uso de AgTx2 como un sonda de la geometría del canal, fue obtener la estructura tridimensional de AgTx2. La síntesis de AgTx2 en forma recombinante permitió obtener miligramos de material purificado para determinar su estructura mediante resonancia magnética nuclear. La determinación de la estructura de AgTx2 fue realizada en el laboratorio del Dr. Gerhard Wagner, escuela de Medicina de la Universidad de Harvard.

Para estudiar la interacción entre AgTx2 y el canal de K^+ *Shaker* se realizaron mutaciones puntuales en ambas proteínas mediante la técnica de mutación sitio-dirigida.

El efecto de estas mutaciones sobre la afinidad de AgTx2 por el canal de K^+ *Shaker* fue cuantificado mediante el registro de corrientes que pasan a través de estos canales expresados en oocitos de *Xenopus laevis*, en presencia y ausencia de AgTx2. Estos estudios funcionales en combinación con el conocimiento de la estructura tridimensional de AgTx2 condujeron al establecimiento de restricciones estructurales para el sitio de unión de AgTx2. Dado que la secuencia de aminoácidos que determina la sensibilidad a AgTx2 es el mismo que contribuye a la formación de la vía de conducción iónica, los datos estructurales obtenidos en este estudio involucran parte del sitio funcional más importante del canal de K^+. Los resultados localizan el extremo amino terminal del segmento que forma la vía de conducción del canal de K^+ *Shaker* entre 12 y 15 Å del eje central del canal y proponen que parte de la secuencia primaria del sitio de unión a AgTx2 posee una estructura de α-hélice.

SUMMARY

K^+ ion channels comprise the most diverse family among ion channels. They are gated in response to membrane potential, G-protein activation, or second messengers such as Ca^{2+}, cAMP. In spite of the diversity of their gating mechanisms all K^+ channels display a strong selectivity for K^+ ions. That is, they are able to exclude Na^+ ions even though Na^+ ions have a smaller crystal radius than K^+ ions.

Full understanding of the molecular basis underlying selectivity in K^+ channels requires the combination of functional studies with structural data. No K^+ channels have yet been purified in large quantities; therefore no structural information by conventional protein structure determination methods is available.

My thesis research focused on the interaction of a recently purified K^+ channel inhibitor from scorpion venom, Agitoxin2 (AgTx2), with the cloned voltage-activated *Shaker* K^+ channel. The ultimate goal is to obtain structural

information on the *Shaker* K^+ channel by using AgTx2 as a caliper for channel geometry.

The first step toward the goal of using AgTx2 as a structural probe of the toxin binding site on the *Shaker* K^+ channel was to synthesize AgTx2 by recombinant methods and to characterize its biophysical properties. The next step was to obtain the three-dimensional structure of AgTx2 for measurement of channel dimensions. AgTx2 was synthesized and milligram quantities of recombinant AgTx2 were purified for the structure determination by nuclear magnetic resonance. The structure of AgTx2 was solved at Dr. G Wagner's laboratory, Harvard Medical School. Lastly, site-directed mutagenesis was used to generate point mutations in both the toxin and the channel. The effects of these mutations on toxin binding were tested by recording the current elicited by the *Shaker* K^+ channel expressed in *Xenopus* oocytes with a two electrode voltage clamp amplifier, in the presence and absence of AgTx2.

The known structure of AgTx2, in addition to the structure-function studies, constrains the molecular architecture of the receptor toxin binding site of the

Shaker K^+ channel. Because the same stretch of amino acids that determines the toxin binding site contributes to the formation of the ion conduction pathway (pore), the structural information obtained pertains to the functionally most important region of K^+ channels, the catalytic unit. The results place the amino-terminal end of the pore forming region of the *Shaker* K^+ channel 12 to 15 Å from the central axis of the channel and suggest an helical conformation for a stretch of amino acids forming the toxin binding site.

Chapter 1

GENERAL INTRODUCTION

The ion channels comprise a class of diverse integral membrane proteins the central function of which is to allow ions to diffuse across otherwise impermeable cell membranes. The movement of ions through channels is involved in a wide range of cellular functions such as volume regulation, sensory transduction, excitation-contraction coupling and secretion. The ion channels are the elementary units directly responsible for cellular electrical excitability and signaling in the nervous system. Ion channels' response (gating) is triggered by different stimuli. According to their gating mechanisms they fall in roughly three categories; ligand-activated, voltage-activated and stretch-activated ion channels.

Voltage-activated ion channels participate in the generation and propagation of action potentials. The

voltage-activated channels are gated in response to changes in the cell membrane electrical potential, and when opened they selectively allow the flow of one kind of ion down its electrochemical gradient. They have been named according to their most important permeant ion as K^+ channels, Na^+ channels, Ca^{2+} channels and Cl^- channels.

K^+ channels are among the most selective channels. Their high selective permeability is remarkable when one considers that they must exclude Na^+ ions, which have a smaller crystal radius than K^+ ions (the permeability ratio Na^+ to K^+ is greatly than 1:100; Hille, 1973). Despite the diversity in their gating mechanisms, Ca^{2+}-activated, G-protein-activated and ATP-sensitive channels all are highly selective for K^+ ions.

Full understanding of how K^+ channels discriminate between K^+ and Na^+ ions requires the identification of the molecular determinants involved in selectivity. The ion conduction pathway, or pore, catalyzes the diffusion of K^+ ions from one side of the membrane to the other.

No K^+ channel has yet been purified in large quantity; thus no direct structural information is available.

Purification has been hindered by the lack of both a natural source rich in K^+ channels and, until recently, high affinity ligands. Even after purification has been achieved, direct structure analysis will be difficult since, at present, membrane proteins are not easily amenable to study by X-ray crystallography.

Two major contributions to our understanding of K^+ channels were the discovery of high affinity ligands (Miller et al., 1985; Garcia et al., 1994; Garcia et al., 1991) and the isolation of a voltage-activated K^+ channel gene (Timpe et al., 1988; Tempel et al., 1987). The combined use of both tools led to a better understanding of what K^+ channels look like.

In the next paragraphs I briefly summarize the studies that contributed enormously to our current picture of K^+ channels.

1. Discovery of high affinity ligands for K^+ channels

Charybdotoxin (ChTx), a basic peptide 37 amino acids in length, was the first K^+ channel inhibitor discovered. ChTx, originally purified from the venom of the scorpion

Leiurus quinquestriatus, specifically inhibits the high-conductance Ca^{2+}-activated K^+ channel with high affinity (nM range; Miller et al., 1985).

The mechanism by which ChTx inhibits the Ca^{2+}-activated K^+ channel was studied in detail by single channel recording. A single toxin molecule binds to the channel on the external side causing blockade of the ion conduction pore. Increasing the K^+ concentration in the internal solution (cytoplasmic face of the channel) causes a non-linear increase in the dissociation rate of ChTx from its binding site. In contrast, the association rate remains unchanged. The enhancement of ChTx dissociation by internal K^+ is voltage-dependent; as membrane potential is varied toward positive values (depolarizing direction) the effect of the internal K^+ is more pronounced. Replacement of the internal K^+ by Na^+ abolishes the voltage dependence. Moreover, the effect of the internal K^+ on ChTx dissociation is valid for other permeant ions and not for impermeant ions. These results show that a toxin bound at the external mouth of the conduction pathway interacts with K^+ ions, coming from the internal side of the channel

(cytoplasmic face). These studies conclude with a model, presented in figure 1.1, of the ChTx block of Ca^{2+}-activated K^+ channel. ChTx prevents ion conduction by physically occluding the channel pore at the external mouth.

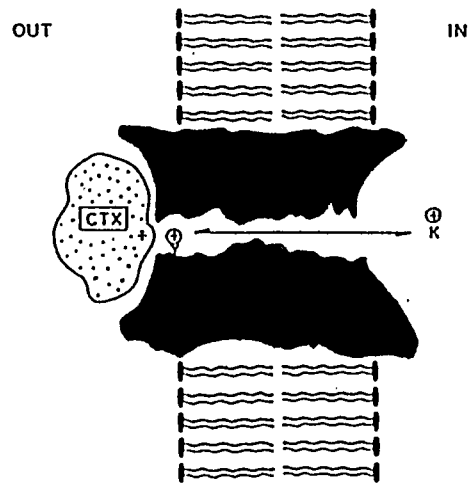

Figure 1.1. ChTx block of the Ca^{2+}-activated K^+ channel. One ChTx molecule blocks ion conduction by occluding physically the outer mouth of the channel pore. A K^+ ion coming from the cytoplasmic face destabilizes a bound ChTx molecule from its binding site. (Figure taken from MacKinnon and Miller, 1988).

The high content of basic residues in ChTx suggests that the toxin may be electrostatically attracted by putative negatively charged groups on the receptor toxin binding site. The dependence of the ChTx association rate, and not dissociation, on the external ionic composition

favors this idea. Increasing the K^+ concentration in the external solution causes a decrease in the association rate. This effect is not specific for a particular cation; Na^+ and organic cations have the same effect (Anderson et al., 1988). In addition, chemical modification of external channel carboxyl groups alters the ion conduction and the ChTx block (MacKinnon et al., 1989; MacKinnon and Miller, 1989b). Moreover, bound ChTx prevents the change in ion conduction upon chemical modification. Therefore, the external surface of the channel indeed carries negatively charged groups that are involved in toxin binding. Together these results are consistent with the existence of an electrostatic component in the toxin-channel interaction.

The discovery of a high affinity ligand that interacts with the most important functional region of the Ca^{2+}-activated K^+ channel, the catalytic unit, opened up new possibilities for studying K^+ channels. The toxin would eventually be used as a probe of the otherwise "obscure" pore of the channel.

The simplest idea behind structure-function studies in proteins is locally to alter the structure and follow the

functional consequence of a particular change. Site-directed mutagenesis is the technique used to substitute a particular amino acid residue on a protein through alteration of the corresponding codon in its DNA sequence.

In order to carry out structure-function studies on the toxin-channel interaction a synthetic ChTx gene was designed to allow the functional expression of ChTx. Recombinant ChTx was synthesized in bacteria as part of a fusion protein and purified (Park et al., 1990). By using recombinant ChTx mutants it was demonstrated that a single toxin residue, lysine at position 27, mediates the interaction between bound toxin and K^+ ions inside the pore (Park and Miller, 1992a). Substitutions of lysine 27 by neutral amino acid residues abolished the voltage dependence of the ChTx dissociation rate. Only toxins with a positive charge at position 27 (lysine or arginine) were destabilized by K^+ ions coming from the internal side.

The solution structure of ChTx was solved by nuclear magnetic resonance (NMR; Bontems et al., 1991b; Bontems et al., 1992). ChTx is a rigid peptide consisting mostly of a triple stranded antiparallel β-sheet and a single α-helix

attached to one side of the β-sheet. Additionally, three disulfide bonds stabilize the structure. ChTx appears to be suitable for site directed mutagenesis studies since its overall well stabilized structure is unlikely to be altered by single point mutations.

The amino acid residues involved in the toxin-channel interaction were identified by mutation of almost every residue in ChTx and measurement of the effect of mutations on the toxin binding (Park and Miller, 1992b; Stampe et al., 1994). For eight amino-acid residues, even conservative mutations altered the dissociation rate constant by a factor greater than eight. These eight residues were considered as functionally crucial and are spatially segregated from the ones which have no effect even upon substitution with a chemically different amino acid. The functionally crucial residues are located on the β-sheet face, which is referred to as the "interaction surface" of the toxin. From the analysis of the interaction surface of the toxin, a rough picture of the receptor toxin binding site was deduced on the basis of complementarity of the contact surfaces in protein-protein interactions.

2. Cloning of a K^+ channel

The cloning of a K^+ channel was the other crucial step in understanding K^+ channels and in obtaining structural information. Because no K^+ channel has yet been purified in large quantities, the cloning strategy was not based on knowledge of the protein product of the gene. A particular *Drosophila* mutant was known to "shake" its legs under ether anesthesia. Functional studies attributed this behavior to the lack of or alteration of a voltage-activated K^+ current. The gene mapped to the *Shaker* locus on the *Drosophila* X chromosome. By chromosome walking, DNA fragments from the *Shaker* locus were obtained and used to screen a cDNA library; transcripts from the cDNA clone were tested for functional expression in oocytes from *Xenopus laevis* to isolate the *Shaker* gene. The *Shaker* locus encoded a transiently voltage-activated K^+ channel denoted the *Shaker* K^+ channel (Timpe et al., 1988; Tempel et al., 1987).

The availability of the *Shaker* K^+ channel clone made possible for the first time structure-function studies on a K^+ channel. The predicted membrane topology based on the

hydropathy profile of the deduced amino acid sequence of the *Shaker* K^+ channel is shown in figure 1.2 (Catterall, 1988; Tempel et al., 1987). The channel comprises six putative transmembrane segments. The amino and carboxy termini are both located on the cytoplasmic side of the membrane. The channel presumably is formed by the assembly of four identical subunits, each containing the six putative transmembrane domains, and arranged about a central pore (a four-fold symmetry axis).

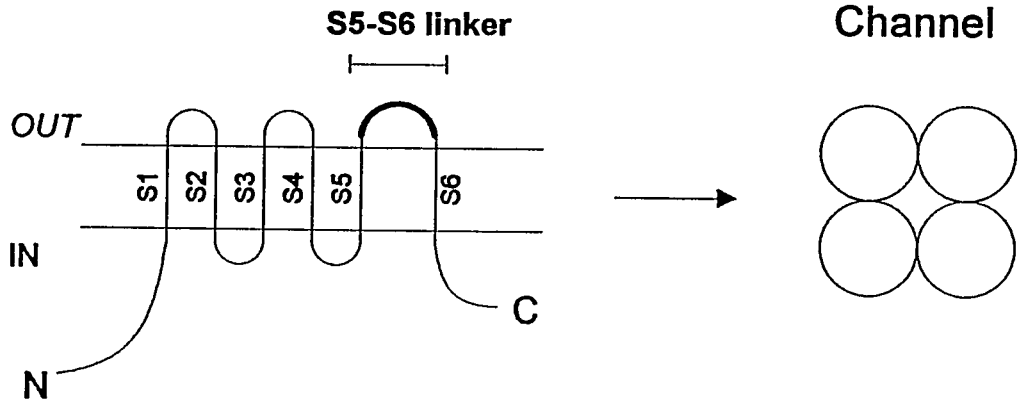

Figure 1.2. Predicted transmembrane topology of the *Shaker* K^+ channel. The hydropathy profile predicted 6 transmembrane spanning regions (S1 to S6). The segment connecting the S5 and S6 transmembrane domain, S5-S6 linker is shown in bold. The channel (right panel) presumably has four-fold symmetry. Each subunit (circles) correspond to one peptide with its 6 transmembrane spanning regions as shown in the left panel.

Native ChTx (ChTx purified from the venom of the scorpion *Leiurus quinquestriatus*) displayed high affinity

for the *Shaker* K^+ channel (MacKinnon et al., 1988; MacKinnon and Miller, 1989a; MacKinnon et al., 1990; MacKinnon, 1991). The known pore-blocking mechanism of ChTx on the Ca^{2+}-activated K^+ channel and the proposed electrostatic component of the toxin-channel interaction was exploited to localize amino acid residues lining the pore of the *Shaker* K^+ channel (MacKinnon and Miller, 1989a; MacKinnon et al., 1990). If the highly basic toxin is indeed attracted to its binding site by negatively charged residues, then neutralization of such residues would affect toxin binding. The negatively charged amino acid residues located on the putative extracellular loops of the *Shaker* K^+ channel were mutated. Out of all the mutated residues only one, at position 422, located in the segment connecting the S5 and S6 transmembrane domain, (S5-S6 linker; figure 1.2 and 1.3), affected toxin affinity (MacKinnon and Miller, 1989a). The effect on the binding energy of charge-altering mutations at position 422, by one unit (substitution with neutral residue) or two units (substitution with positively charged residue), was well described by Coulomb's law. Additionally, mutations that

conserved the negatively charged residue at 422 showed no effect on toxin affinity. Therefore, channel residue 422 stabilizes the toxin in its binding site via a through-space electrostatic interaction. Consequently, residue 422 is located near the toxin binding site and resides on the external mouth of the channel pore, where the toxin is known to bind.

Further mutational analysis of the S5-S6 linker of the *Shaker* K^+ channel identified several other residues that affect toxin binding in one of two different ways, through electrostatic mechanisms or through possible steric effects (MacKinnon et al., 1990).

In conclusion, the effect of mutations on toxin binding allowed the identification of the S5-S6 linker of the *Shaker* K+ channel as forming part of the external mouth of the channel pore.

The same mutational analysis approach was applied to identified channel residues lining the narrow part of the pore. For this purpose, a smaller channel blocker such as tetraethylammonium ion (TEA) was used as a probe rather than toxin. Residues on the S5-S6 linker affecting TEA

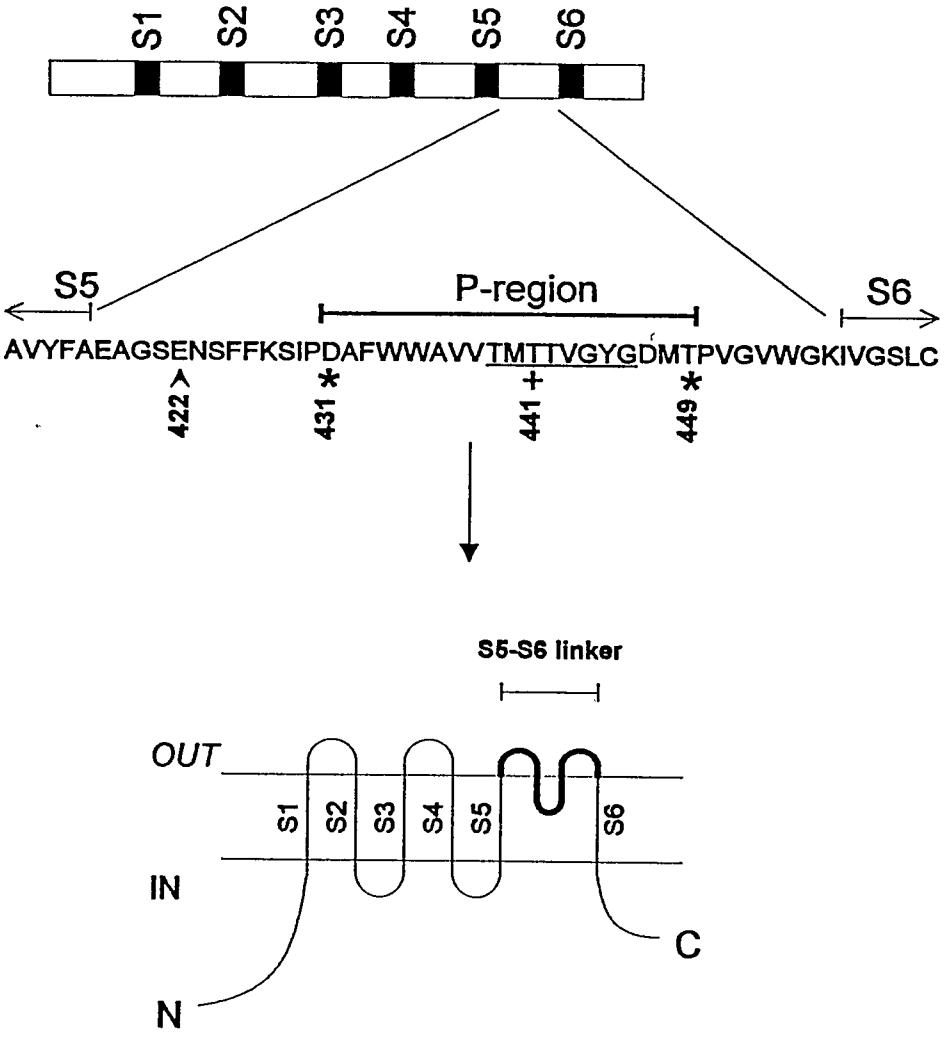

Figure 1.3. Current model of the membrane topology and partial amino acid sequence of the *Shaker* K^+ channel. The hydropathy profile predicts 6 transmembrane spanning regions (S1 to S6; figure 1.2). Structure-function studies place the segment connecting the S5 and S6 transmembrane domains (S5-S6 linker) as partially dipping into the plane of the membrane. The functionally important regions for external TEA binding (*), internal TEA binding (+) and toxin binding (^) are shown. The K^+ channel signature sequence is underlined.

block applied on the internal (cytoplasmic) or the external (extracellular) face of the channel were identified by site-directed mutagenesis (figure 1.3; MacKinnon and Yellen, 1990; Yellen et al., 1991). At two positions, 431 and 449, external TEA affinity was altered while internal TEA affinity remained unchanged. However, the effect of mutating residue 449 on TEA affinity is more than one order of magnitude larger than the effect at position 431. The internal TEA affinity was altered upon mutation of residue 441. The external TEA affinity was insensitive to mutation at 441. Because residue 441 is approximately in the middle of the segment between 431 and 449, at least part of the segment after residue 431 must enter the plane of the membrane and reappear again on the external side at position 449.

Experiments with chimeric channels provided independent evidence for the association of a linear segment in the S5-S6 linker in the formation of the ion conduction pathway. A 21 amino acid segment of the S5-S6 linker was exchanged between related voltage-activated K^+ channels that differ in their conduction properties and TEA

blockade. The chimeric channel acquired the conduction properties and TEA affinity characteristics of the channel donor of the the S5-S6 linker segment (Hartmann et al., 1991). Additionally, point mutations in the S5-S6 linker of an alternatively spliced *Shaker* K^+ channel were shown to alter the ionic selectivity (Yool and Schwarz, 1991).

Altogether, the above studies and other additional studies defined a linear amino acid sequence, between residues 431 and 449, lining the ion conduction pathway. The segment between amino acid 431 and 449 (*Shaker* K^+ channel numbering), is usually referred to as the pore-forming region or P-region in voltage-activated K^+ channels (figure 1.3; MacKinnon and Miller, 1989a; MacKinnon et al., 1990; MacKinnon and Yellen, 1990; Yellen et al., 1991; Yool and Schwarz, 1991; Hartmann et al., 1991; Heginbotham and MacKinnon, 1992; Heginbotham et al., 1992; Kavanaugh et al., 1991; Kavanaugh et al., 1992; Kirsch et al., 1992; De Biasi et al., 1993).

Further evidence had confirmed that residues in the S5-S6 linker determine ion selectivity. On the basis of sequence comparison between the S5-S6 linker of voltage-

activated K^+ channels and cyclic nucleotide-gated ion channels, mutant K^+ channels were designed which displayed several ion conduction properties of cyclic nucleotide-gated channels, including the lack of discrimination between Na^+ and K^+ ions (Heginbotham et al., 1992). These results suggest, even if in an unknown way, that the S5-S6 linker is involved in the formation of the selectivity filter of K^+ channels. This idea had firmly been supported by mutagenesis studies on a short stretch of eight amino acids located in the previously defined P-region, which are extremely conserved among K^+ channels. This region has been called the K^+ channel signature sequence (Heginbotham et al., 1994).

Other regions of the voltage-activated K^+ channels, such as the S4-S5 loop and the S6 segment had also been shown to affect K^+ permeation (Jan and Jan, 1994; Choi et al., 1993; Slesinger et al., 1993; Lopez et al., 1994); however, most of the evidence favors the P-region as the main determinant of K^+ selectivity in the ion conduction pathway.

To date, a great diversity of K^+ channels has been cloned including a Ca^{2+}-activated K^+ channel (Anderson et al., 1992; Atkinson et al., 1991; Baumann et al., 1988; Bruggemann et al., 1993; Butler et al., 1989; Butler et al., 1993; Frech et al., 1989; Ho et al., 1993; Kamb et al., 1988; Kubo et al., 1993a; Kubo et al., 1993b; Pak et al., 1991; Pongs et al., 1988; Schachtman et al., 1992; Sentenac et al., 1992; Tempel et al., 1987; Warmke et al., 1991; Wei et al., 1990; Yokoyama et al., 1989). Sequence alignment of different cloned K^+ channel reveals the highest degree of identity between the fifth and the sixth putative transmembrane segments, the S5-S6 linker (Agus et al., 1989; Jan and Jan, 1990; Heginbotham et al., 1994). Also, other K^+ channel inhibitors, collectively called scorpion toxins, that are closely related to ChTx, have been purified (Garcia et al., 1991; Gimenez-Gallego et al., 1988; Galvez et al., 1990; Lucchesi et al., 1989). The mechanism of inhibition of the new scorpion toxins is known to be the same pore-blocking mechanism described for ChTX on the Ca^{2+}-activated K^+ channel (Candia et al., 1992; Giangiacomo et al., 1992).

Chimeras between toxin sensitive and toxin insensitive K^+ channels demonstrated that the main linear component that determines the receptor toxin binding site in voltage-activated K^+ channels is the S5-S6 linker. Toxin sensitivity was transferred with the S5-S6 linker from toxin sensitive to toxin insensitive K^+ channels (Gross et al., 1994).

3. Specific *Shaker* K^+ channel inhibitors.

The experiments described in the previous section were carried out with native ChTx. In contrast, chemically synthesized ChTx exhibited an unexpectedly low affinity for the *Shaker* K^+ channel (Oliva et al., 1991). Therefore, other components in the native ChTx preparation must account for the activity observed against the *Shaker* K^+ channel. This finding motivated the search for high affinity inhibitors from scorpion venom specifically directed against the *Shaker* K^+ channel.

Three new peptide inhibitors, Agitoxin 1, 2 and 3 (AgTx 1, 2 and 3), were purified on the basis of their affinity for the *Shaker* K^+ channel (Garcia et al., 1994).

Agitoxins are 38 amino acids in length and are related in their amino acid sequence to ChTx and other scorpion toxins. However, on the basis of their sequence alignment, AgTxs fall in a different class from ChTx.

Although the scorpion toxins exhibit some overlap in their receptor specificity, they tend clearly to differentiate between Ca^{2+}-activated K^+ channels and voltage-activated K^+ channels. Agitoxins appear to block specifically the *Shaker* K^+ channel and many of its mammalian homologues. However, *Shaker* K^+ channels with a single substitution, Phe425 with Gly (F425G), on a residue located in the S5-S6 linker of the *Shaker* K^+ channel increases the ChTx affinity by 3 orders of magnitude, to the picomolar range (Goldstein and Miller, 1993). Complementary mutagenesis on the toxin and the channel suggests that Phe425 causes steric hindrance which prevents strong binding of ChTx to the wild-type *Shaker* K^+ channel.

The present thesis describes studies on the interaction of these new high affinity peptides with the *Shaker* K^+ channel. The ultimate goal was to obtain

structural information on the outer mouth of the ion conduction pathway of a cloned K^+ channel.

For presentation, this work has been divided into chapters. The second chapter describes the methodology used to synthesize recombinant AgTxs from the gene to the protein and the electrophysiological characterization of these toxins. The third chapter describes the characteristics of the solved three-dimensional structure of AgTx2. The fourth chapter describes a new approach developed to assign the spatial location of amino acid residues in the S5-S6 linker of the *Shaker* K^+ channel with respect to the known AgTx2 structure. The fifth and last chapter describes further applications of the methodology.

Altogether this work has placed strong spatial constraints on amino acids in the P-region of the *Shaker* K^+ channel which must be incorporated in future structural models.

Chapter 2

SYNTHESIS AND CHARACTERIZATION OF THREE INHIBITORS OF VOLTAGE-DEPENDENT K^+ CHANNELS FROM *LEIURUS QUINQUESTRATUS* VAR. *HEBRAEUS* VENOM

Agitoxins purified from scorpion venom were described as potent inhibitors of the *Shaker* K^+ channel and other related voltage activated K^+ channels. The suitability of using AgTxs as structural probes of the pore-forming region of the *Shaker* K^+ channel depends on the possibility of being genetically manipulated. This was achieved by the design of an AgTx gene capable of being expressed in bacteria as a fusion protein. Because of the limited quantities of purified native toxin, all the biophysical characterization of the AgTxs block of the *Shaker* K^+ channel was done with recombinant AgTxs.

The amino acid sequences determined for the purified native AgTxs 1, 2 and 3 are shown in figure 2.1 (Garcia et al., 1994). Agitoxins are 38 amino acids in length and have

no tryptophan or tyrosine residues. Therefore they are not detectable by UV absorption at 280 nm. AgTx2 differs from AgTx1 by four amino acid residues at positions 7, 15, 29 and 31. AgTx3 differs from AgTx2 in a single residue at position 7.

```
                1   5   10   15   20   25   30   35
                ↓   ↓   ↓    ↓    ↓    ↓    ↓    ↓
AgTx1     GVPINVKCTGSPQCLKPCKDAGMRFGKCINGKCHCTPK

AgTx2     GVPINVSCTGSPQCIKPCKDAGMRFGKCMNRKCHCTPK

AgTx3     GVPINVPCTGSPQCLKPCKDAGMRFGKCINGKCHCTPK
```

Figure 2.1. Amino acid sequence of Agitoxins. The arrows correspond to the residues numbered above the AgTx1 sequence. The amino acid differences between AgTx1 and AgTx2 are shown in bold on the AgTx2 sequence. AgTx3 differs from AgTx2 in one residue (shown double underlined on the AgTx3 sequence). The amino-acid sequence determination was done at Merck Research Laboratories as follow: the purified sample was reacted with iodoacetic acid and the alkylated toxin purified by reversed-phase HPLC. The toxin was digested with endoproteinase Lys-C, and the fragments were purified by reversed-phase HPLC. Amino-terminal Edman degradation was performed using a Porton 2090 microsequencer.

Two of the three AgTxs, AgTx1 and AgTx2, were synthesized by recombinant methods. The synthesis of recombinant AgTxs is described below, starting from the designing of the gene and followed by the electrophysiological characterization which demostrates

their identities as active components against the *Shaker* K^+ channel.

METHODS

K^+ Channel mutagenesis and expression.

Shaker K^+ channel clone was in a Bluescript vector (Stratagene, La Jolla, CA). The clone used in these studies contains a deletion of residues 6 to 46 in order to remove the fast inactivation domain of the *Shaker* K^+ channel (*Shaker* IR, or inactivation removed; Hoshi et al., 1990). Otherwise it exhibits the same characteristics as the *Shaker* K^+ channel. The modification facilitated electrophysiological recording. Mutant channel clones, E422K, T449K and D431N, were available in the laboratory. All channel mutations were carried out by complementary strand synthesis (Kunkel, 1985). The mutant clones were selected by dideoxy DNA sequencing (Sanger et al., 1977). The vector was linearized with Hind III and in vitro transcribed using T7 polymerase. The cRNA was expressed in Xenopus oocytes, stage VI, by microinjection (Mackinnon et al., 1988). *Xenopus laevis* were anesthetized by cooling on ice before removal of the oocytes by surgery. The oocytes were defolliculated by incubation with collagenase (3mg/ml)

for 1.5-2 hours, at room temperature (21-23 °C), in Ca^{2+}-free solution containing in millimolar: 82.5 NaCl, 2.5 KCl, 1 $MgCl_2$, 5 Hepes, pH 7.6 (NaOH). After the collagenase treatment, the oocytes were rinsed repeatedly (4-6 times) and stored at 18 °C in buffer solution containing in millimolar: 96 NaCl, 2 KCl, 1.8 $CaCl_2$, 1 $MgCl_2$, 5 Hepes, pH 7.6 (NaOH) plus gentamycin (50 µg/ml).

Electrophysiological recording.

The K^+ currents were recorded using a two-microelectrode voltage clamp amplifier (Warner instruments) operated under computer control. Channels were expressed to a level of 0.5 to 1.5 µA (correponding to 1-2 days after injection) of current elicited during a 50 ms depolarizing step from a holding potential of -70 mV to 0 mV. The oocytes were continously perfused with buffer (containing in millimolar 96 NaCl, 2 KCl, 0.3 $CaCl_2$, 1 $MgCl_2$, 5 Hepes, pH 7.6 (NaOH), (control records). The toxin at a given concentration was added to the buffer just before perfusion through a separated perfusion line. To minimize nonspecific sticking of toxin to the recording chamber and

perfusion lines 50 µg/ml of bovine serum albumin was added along with the toxin. The corresponding AgTx was removed after reaching equilibrium to demostrate full recovery from blockade. On the case of AgTx1 this was not feasible because its dissociation rate is very slow (more than 15 minutes). All experiments were carried out at room temperature, 21-23 °C.

RESULTS

Construction of the AgTx1 gene

The first gene constructed was the gene coding for AgTx1. The gene encoding AgTx2 was constructed by PCR amplification of the AgTx1 gene using mutant oligonucleotides as primers.

The AgTx1 gene was synthesized as described by Park and Miller (Park et al., 1990). The general strategy followed in constructing the AgTx1 gene is depicted in figure 2.2A. A nucleotide sequence deduced from the amino-acid sequence was designed to encode AgTx1 (figure 2.2B). Four overlapping oligonucleotides, which together encode AgTx1 (see figure 2.2) were chemically synthesized, purified, phosphorylated and ligated. For the subsequent cloning, the AgTx1 gene generated in these way included two flanking restriction sites, Sal I and Hind III. The toxin was intended to be produced in bacteria as a fusion protein with T7gene9 bacteria protein, therefore, a specific recognition site for protease cleavage was included at the

A.

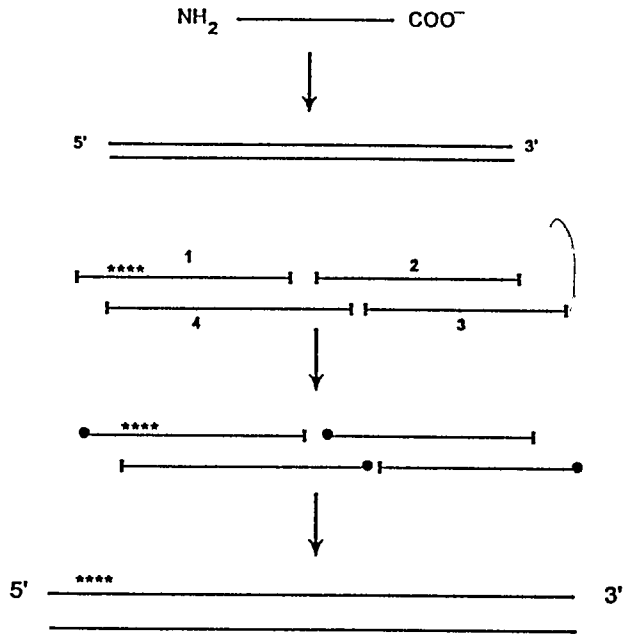

B.

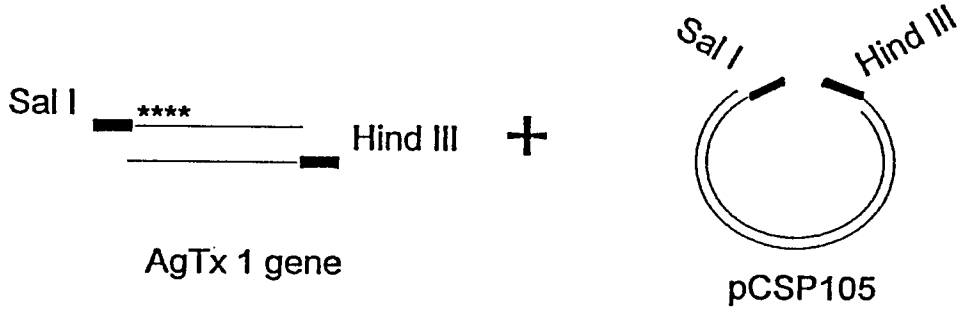

Figure 2.2. (A and B). General strategy for the construction and expression of the AgTx1 gene. A. Two overlapping oligonucleotide duplexes were designed according to the AgTx1 nucleotide sequence deduced from the amino-acid sequence of AgTx1. The four oligonucleotides (labeled 1 to 4, see sequence below) were chemically synthesized on an Applied Biosystems model 391 DNA synthesizer and purified, phosphorylated, annealed and ligated together. The synthetic AgTx1 gene containing the flanking restriction sites Sal I and Hind III was inserted as a cassette into the pCSP105 vector (kindly provided by Park and Miller at Brandeis). The sequence of the synthetic AgTx1 gene was confirmed by dideoxy sequencing across the Sal I Hind III cassette. The filled circles represent a phosphate group. The stars show the enteropeptidase recognition site. B. The synthetic AgTx1 gene was ligated to the pCSP105 vector (see figure 2.3) previously digested with SalI and Hind III.

C.

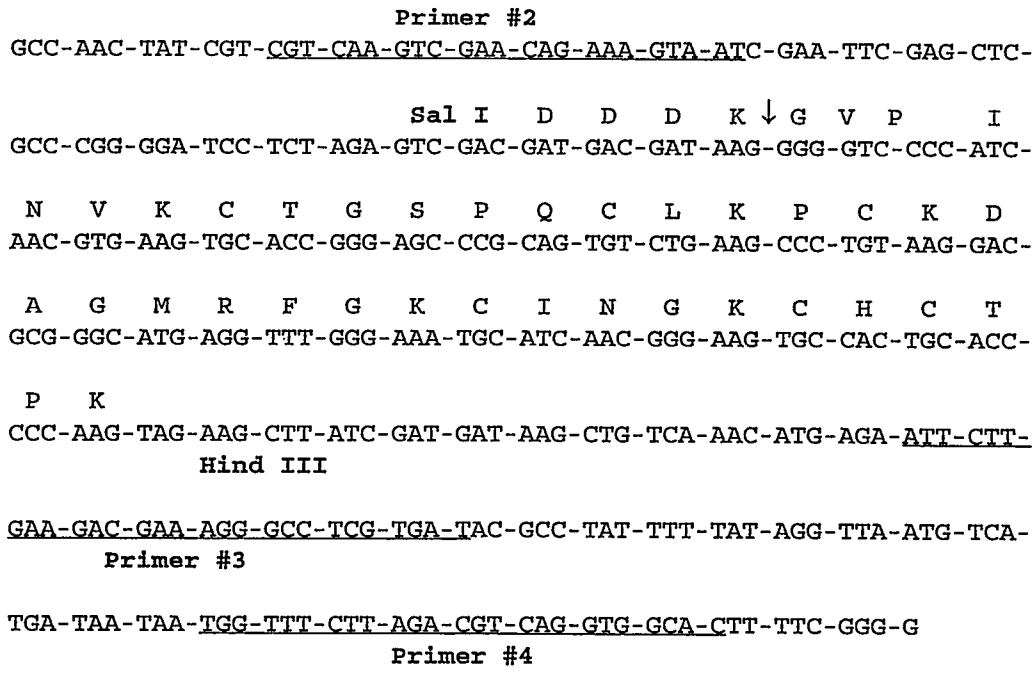

Figure 2.2. C. Nucleotide sequence for the synthetic AgTx1 gene and its flanking regions. The encoded amino acid sequence is shown (single letter code). The AgTx1 gene corresponds to the sequence flanked by the SalI and Hind III restriction sites. The arrow shows the enteropeptidase recognition site (DDDK linker). The primers #2, 3 and 4 are used as flanking primers for PCR. 1) 5'TC-GAC-GAT-GAC-GAT-AAG-GGG-GTC-CCC-ATC-AAC-GTG-AAG-TGC-ACC-GGG-AGC-CCG-CAG-TGT-CTG-AAG 3'. 2) 5'CCC-TGT-AAG-GAC-GCG-GGC-ATG-AGG-TTT-GGG-AAA-TGC-ATC-AAC-GGG-AAG-TGC-CAC-TGC-ACC-CCC-AAG-TAG-A 3'. 3) AG-CTT-CTA-CTT-GGG-GGT-GCA-GTG-GCA-CTT-CCC-GTT-GAT-GCA-TTT-CCC-AAA-CCT-CAT-GCC-CGC-GTC-CT 3'. 4) 5' T-ACA-GGG-CTT-CAG-ACA-CTG-CGG-GCT-CCC-GGT-GCA-CTT-CAC-GTT-GAT-GGG-GAC-CCC-CTT-ATC-GTC-ATC-G 3'.

amino terminal end of the coding region. The cleavage site corresponds to the amino acid sequence Asp-Asp-Asp-Lys (DDDK in single letter code) which is specifically recognized by enteropeptidase.

The original pCSP105 vector (kindly given by Park and Miller at Brandeis, see figure 2.2A and 2.3), which contains the ChTx gene between flanking sites for Sal I and Hind III, was digested with Sal I and Hind III, and the synthetic AgTx1 gene was inserted in place of ChTx as a cassette (figure 2.2A).

The final expression vector, pCSP105-AgTx1, is shown in figure 2.3. The DNA sequence for the synthetic AgTx1 gene was confirmed by dideoxy sequencing between the flanking sequences Sal I and Hind III.

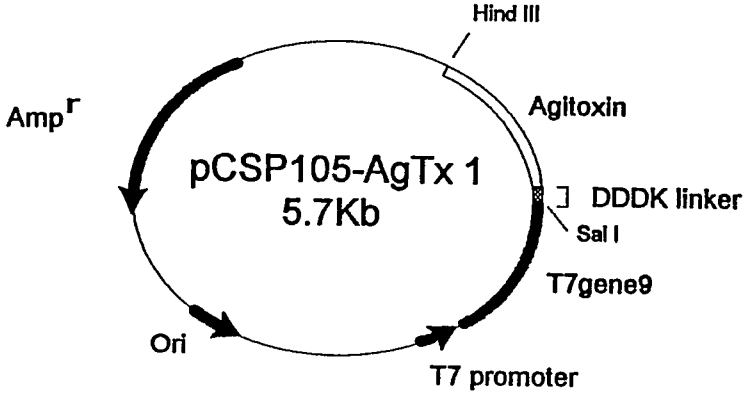

Figure 2.3. The expression vector for AgTx1. The vector is designed to express a T7gene9-DDDK-AgTx1 fusion protein. The AgTx1 gene was inserted into SalI and Hind III sites of the pCSP105 original vector. The coding region for AgTx1 is solid white and the enteropeptidase recognition site is hatched. Amp^r, ampicillin resistance; ori, origin of replication.

Construction of the AgTx2 gene

The AgTx2 gene was constructed from the AgTx1 gene by PCR amplification using the pCSP105-AgTx1 plasmid as template and primers #2 and #4 as flanking primers (figure 2.2C). Two primers were designed, each containing two amino-acid substitution, which in total account for the four amino acid differences between Agtx1 and 2 (figure 2.1). One primer contains the Lys to Ser at position 7 and Leu to Ile at position 15 substitutions. The other primer contains the Ile to Met at position 29 and Gly to Arg at position 31 substitutions. Two independent PCR reaction were carried out, one for each primer with the corresponding flanking primer. Each PCR product was gel purified and used as a primer to carry out a second PCR reaction which covered the entire AgTx2 gene. The product of the second PCR reaction was phenol extracted, precipitated and digested with Sal I and Hind III. The Sal I-Hind III fragment was gel purified and inserted as a cassette into the pCSP105 vector. The confirmation of the AgTx2 sequence was done by dideoxy DNA sequencing between the flanking sequences Sal I and Hind III.

Expression and purification of recombinant AgTx

The expression and purification of both, AgTx1 and AgTx2 was performed essentially as described (Park et al., 1990; Garcia et al., 1994). *E.coli* DH1 was used for plasmid propagation and DE-3 (BL-21) for the expression of the fusion protein containing the toxin (gene9-DDDK-AgTx). *E. coli* DE-3 harboring the pCSP105-AgTx vector were cultured at 37°C in rich LB media in the presence of 100 ug/ml of ampicillin. The cells were induced to produce fusion protein under the control of the T7 promoter by adding 1 ml/l of 0.5 mM isopropyl β-D-thiogalactoside (IPTG). After 2-2.5 hours the cells were harvested by centrifugation, washed with extraction buffer (containing in millimolar: 10 tris-HCl pH.8, 50 NaCl and 2 Na-EDTA) and the pellet stored at -70°C. The cells were sonicated, and the isolation of the fusion protein was carried out by ion exchange chromatography. The toxin sample was loaded onto a diethylaminoethyl cellulose (DE-52) column previously equilibrated with buffer containing in mM: 50 Tris-HCl pH.7, 50 NaCl and 5 2-β-mercaptoethanol. The fusion protein was fractionated by using a 50 to 500 mM NaCl linear

gradient. Fractions containing the fusion protein were identified by Coomassie stained SDS-PAGE gels, combined and dialyzed overnight against 10 mM Tris-HCl and 0.5 mM 2-β-mercaptoethanol, pH 7. The toxin was cleaved from the fusion protein by incubation for 23 to 32 hours at 37 °C with enteropeptidase (200 U/mg of fusion protein) along with 5 mM $CaCl_2$. The extinction coefficient used for the fusion protein was 1 mg/A_{280}. The toxin was purified from the fusion protein also by ion exchange chromatography (SP sephadex). After washing the column with 10 mM NaOH and 150 mM NaCl solution it was equilibrated with buffer containing, in millimolar, 50 NaCl, 10 Na-borate and 10 Na_2CO_3, pH 9.0 and eluted with a pH step from 9.0 to 12.0 (buffer containing in mM, 20 NaCl, 10 Na_2HPO_4 and 10 Na_2CO_3). After adjust the pH of the toxin sample to approximately 6.0, the sample was loaded onto a C_8 reversed-phase HPLC. Mobile phase A was 0.1% trifluoroacetic acid in H_2O and mobile phase B contained 10% isopropanol and 5% acetonitrile in H_20. Toxin was eluted using the following gradient; 0-35% mobile phase B in 2 minutes, then 35-90%B in 40 minutes and 90 to 100%B in

20 minutes. Figure 2.4 shows an HPLC profile of a recombinant toxin fraction eluted from the SP sephadex column. Under this conditions recombinant AgTx2 appear as a single peak, more than 90% pure.

Individual peaks were collected, lyophilized and stored at -20 °C. The final yield was 0.6-1.2 mg of toxin per liter of bacteria culture. Verification of the identity of the purified material was done by mass spectrometry and amino acid analysis (Table 1).

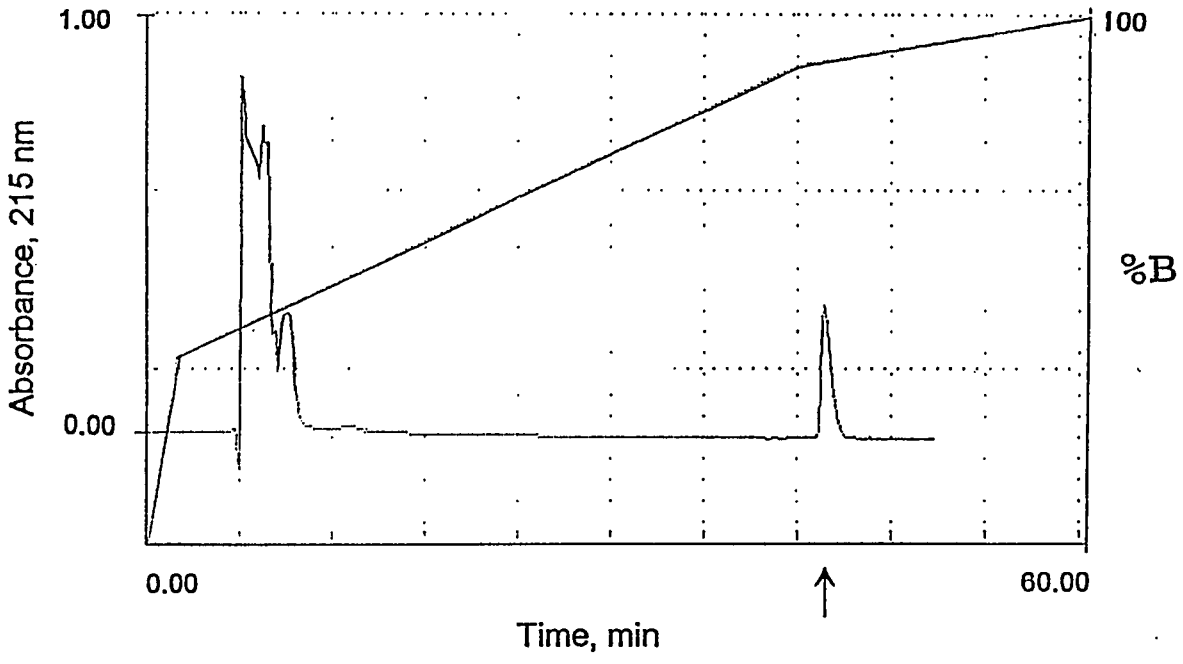

Figure 2.4. Reversed-phase HPLC of an AgTx2 fraction. A fraction eluted from the sephadex column was loaded (following pH adjustment to 6.0) onto a C_8 reversed-phase HPLC column. Mobile phase A contained 0.1% trifluoroacetic acid in H_2O and mobile phase B contained 10% isopropanol and 5% acetonitrile in H_20. Toxin was eluted using the following gradient; 0-35% mobile phase B in 2 minutes, then 35-90%B in 40 minutes and 90 to 100%B in 20 minutes. The arrow indicate the AgTx2 peak.

	residues/mol of toxin			
	$AgTX_1$		$AgTX_2$	
	obs	int	obs	int
aspartic acid, asparagine	2.85	3	2.63	3
glutamic acid, glutamine	0.99	1	0.98	1
serine	0.99	1	1.77	2
glycine	4.77	5	4.06	4
histidine	0.95	1	0.95	1
arginine	1.03	1	2.08	2
threonine	1.86	2	2.06	2
alanine	0.98	1	1.06	1
proline	3.77	4	3.99	4
tyrosine	ND[b]		ND	
valine	1.90	2	1.96	2
methionine	1.05	1	1.73	2
cysteine	5.82	6		
isoleucine	1.85	2	1.73	2
leucine	0.99	1	ND	
phenylalanine	0.99	1	0.98	1
lysine	5.77	6	6.05	6

Table 2.1. Amino acid analysis of recombinant AgTx1 and AgTx2. The amino acid analysis was done at the the Biopolymers Facilities, Harvard Medical School with the sample purified as described in the text. ND, not detected.

Inhibition of *Shaker* K^+ channels by AgTxs

The ability of recombinant AgTx1 and 2 to inhibit the ionic current passing through the *Shaker* K^+ channel was tested in oocytes of *X.laevis* expressing the *Shaker* K^+ channel. Current was recorded using a two-microelectrode voltage clamp amplifier. The inhibition of the K^+ current elicited by voltage steps from a holding potential of -80 mV to 0 mV is fully reversible as shown figure 2.5A. The

time course is given in figure 2.5B. The fraction of unblocked current that remains after the application of various toxin concentrations is shown in figure 2.5C. The inhibition equilibrium constant (K_i) was obtained from these dose-response curves for AgTx1, AgTx2 and for ChTx. The K_is obtained for AgTx1 and AgTx2 are 0.16 nM and 0.64 nM, respectively. In contrast, the *Shaker* K^+ channel exhibits a significantly lower sensitivity to ChTx (K_i = 227 nM). These results confirm the low affinity of synthetic ChTx for the *Shaker* K^+ channel previously described (Oliva et al., 1991).

The studies in which ChTx was thought to be the active component responsible for *Shaker* K^+ channel inhibition were also carried out on *Shaker* K^+ channels with point mutations (MacKinnon and Miller, 1989a; MacKinnon et al., 1990). In order to test if AgTx2 accounts for the activity against the *Shaker* K^+ channel in those studies, AgTx2 was tested against the same mutant channels. AgTx2 was used initially because its kinetics resembled those previously observed and because AgTx1 has a very slow dissociation rate (data not shown).

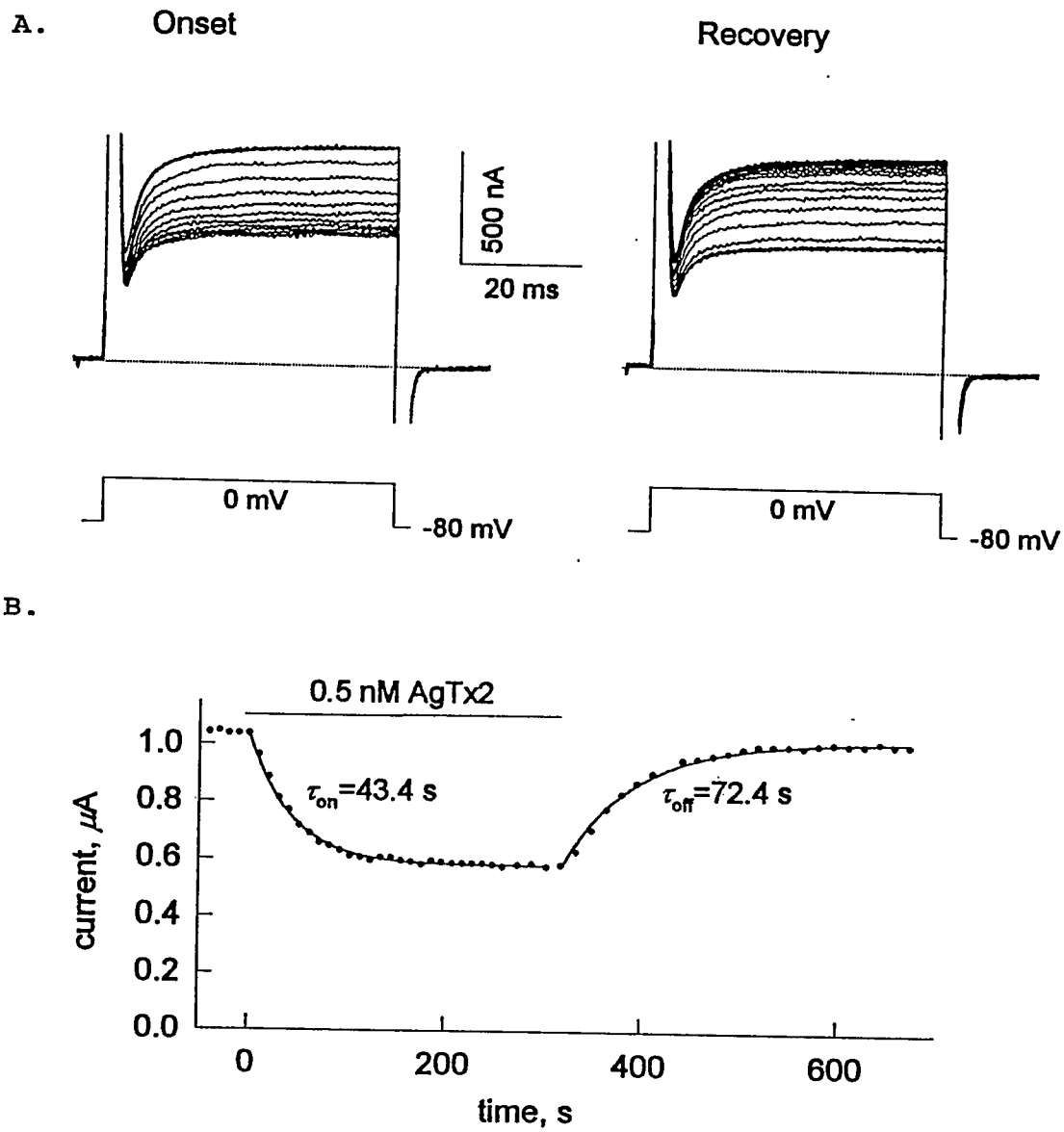

Figure 2.5. (A and B). Inhibition of *Shaker* K^+ channels by Agitoxins. A. *Shaker* K^+ channels were expressed in *Xenopus* oocytes. Current elicited by voltage steps of 50 ms duration from a holding potential of -80 mV to 0 mV are recorded by two-electrode voltage clamp. After 5 traces were recorded in the absence of toxin (control solution), solution containing 0.5 nm AgTx2 was perfused. The switch of perfusion lines was done by computer controlled solenoides valves. Once equilibrium blockade was reached toxin was removed by perfusing with control solution. The inhibition is fully reversed upon removal of the toxin. B. Time course of current. The solid curves correspond to single exponential fits with t_{on} = 43.4 sec and t_{off} = 72.4 sec.

C.

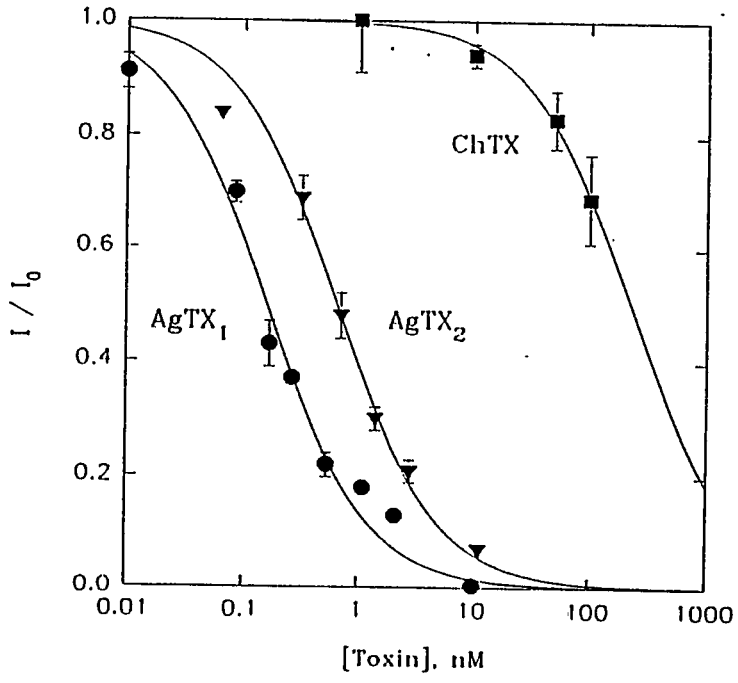

Figure 2.5. C. The fraction of unblocked current, I/I_o, is plotted as a function of toxin concentration for AgTx1 (circles), AgTx2 (triangles) and ChTx (squares). Curves through the data points (least-squares fit) correspond to $I/I_o = K_i/(K_i + [Tx])$, where [Tx] is the toxin concentration and K_i is the inhibition constant for the given toxin. Ki = 0.16, 0.64 and 227 nM for AgTx1, AgTx2 and ChTx, respectively. Each point is the mean ± SE (or range of mean) of 2 to 7 separate measurements.

Figure 2.6 shows dose-response curves for three different channel mutants at residues on the S5-S6 linker, the amino-acid segment forming the binding site for the presumed ChTx. The single substitution of Asp431 with Asn (D431N) or of Thr449 with Lys (T449K) confers toxin insensitivity. In contrast, when Glu422 is substituted with a Lys (E422K), the toxin affinity decreases by a factor of

14. These results are quantitatively consistent with AgTx2 being the component which accounts for the activity against the *Shaker* K^+ channel observed in past studies using purified ChTx preparations.

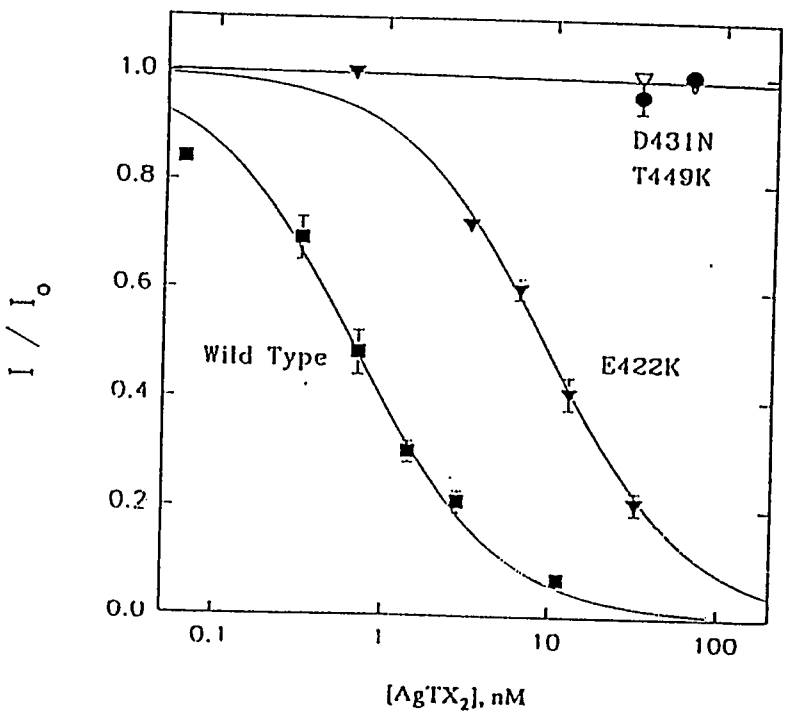

Figure 2.6. Effect of *Shaker* K^+ channel mutations on inhibition by AgTx2. The fraction of unblocked current, I/I_o is plotted as a function of AgTx2 concentration for the wild-type *Shaker* K^+ channel (squares) and channel with point mutations, E422K (filled triangles), D431N (circles) and T449K (empty triangles). The inhibition constants for the wild-type and the E422K channel is 0.64 and 9.1 nM, respectively. Mutants D431N and T449K are insensitive to AgTx2 over the range tested. Recordings were perfomed as described in figure 2.5. Each point is the mean ± SE (or range of mean) of 2 to 7 separate measurements.

DISCUSSION

The Agitoxins are related in their amino acid sequence to ChTx and other known K^+ channel inhibitors from scorpion venom. The common feature of these toxins is their high content of basic residues, lysines and arginines, as well as the presence of six cysteine residues. Agitoxins also exhibit unique features such as the characterisic starting sequence of three amino acids, Gly-Val-Pro, at the amino terminal end of the peptide and the high content of proline residues.

On the basis of the alignment of their amino acid sequences with respect to the six cysteines, the scorpion toxins fall into three subclasses (figure 2.7). Subclass I, ChTx (Gimenez-Gallego et al., 1988), IbTx (Galvez et al., 1990) and Lq2 (Lucchesi et al., 1989); subclass II, NxTx (Possani et al., 1982) and MgTx (Garcia-Calvo et al., 1993), and finally class III comprising the new class described in this chapter, AgTxs (Garcia et al., 1994), and Ktx (Romi et al., 1993; see figure 2.7 legend for abbreviations). The amino acid identity between members of

each subclass is greater than 70% while between members of different subclasses identity is less than 50%.

		3th	4th
Class I.			
ChTx	Z F T N V S C T T S K E C W S V C Q R L H N T S R G		K C M N K K C R C Y S
IbTx	Z F T D V D C S V S R E C W S V C K D L F G V S R G		K C M G K K C R C Y Q
Lq2	Z F T Q E S C T A S N Q C W S I C K R L H N T N R G		K C M N K K C R C Y S
Class II.			
NxTx	T I I N V K C T S P K Q C S K P C K E L Y G S S A G A	K	C M N G K C K C Y N N
MgTx	T I I N V K C T S P K Q C L P P C K A Q F G Q S A G A	K	C M N G K C K C Y P H
Class III.			
AgTx1	G V P I N V K C T G S P Q C L K P C K D A	G M R F G	K C I N G K C H C T P K
AgTx2	G V P I N V S C T G S P Q C I K P C K D A	G M R F G	K C M N R K C H C T P K
AgTx3	G V P I N V P C T G S P Q C I K P C K D A	G M R F G	K C M N R K C H C T P K
KTX	G V E I N V K C S G S P Q C L K P C K D A	G M R F G	K C M N R K C H C T P K

Figure 2.7. Sequence alignment of different K^+ channel inhibitors from scorpion venom. The sequences have been aligned with respect to the six cysteine residues (shown in bold). The K^+ channel inhibitors can be classified into three subclasses on the basis of their amino acid sequences. ChTx,Charybdotoxin; IbTx, Iberiotoxin; Lq2, *Leiurus quinquestriatus2*; NxTx,Noxiustoxin; MgTx, Margotoxin; AgTx, Agitoxins. The conserved residue among all the toxins, Lys 27, is shown outlined. Notice that the length between the third and fourth cysteine (numbered above ChTx sequence) is not conserved among toxins of different subclasses.

Mutagenesis studies on the stretch of amino acid that mainly determines the toxin binding site on K^+ channels (S5-S6 linker) support the idea that different K^+ channels share a common toxin binding site. Although there is overlapping receptor specificity, it is clear that the members of the subclass I toxins but not subclass II or III toxins are high affinity blockers for Ca^{2+}-activated K^+ channels (Garcia et al., 1991). On the other hand, the agitoxin family members are highly selective for voltage-activated K^+ channels. However, KTx which is closely related to agitoxins, has been reported as blocker of the high-conductance Ca^{2+}-activated K^+ channels in molluscan neurons (Romi et al., 1993).

The most extensively studied member of the K^+ channel inhibitors from scorpion venom is ChTx, the solution structure of which has been solved (Bontems et al., 1991b; Bontems et al., 1992). Mutagenesis studies have identified the functionally critical residues for the interaction between ChTx and the Ca^{2+}-activated K^+ channel (Stampe et al., 1994) and also between ChTx and the *Shaker* K^+ channel with a point mutation (F425G) that confer high sensitivity

to ChTx (Goldstein et al., 1994). All of these residues lie on the surface formed by the β-sheet on the ChTx structure, known as the toxin interaction surface. Conservative substitution of the critical residues weaken toxin affinity by at least 8-fold. Only one of these residues, Lys27, is fully conserved among all the known K^+ channel inhibitors from scorpion venom (figure 2.7). Lys27 on ChTx has been shown to interact directly with K^+ ions inside the ion conduction pore of the Ca^{2+}-activated K^+ channel (MacKinnon and Miller, 1988; Park and Miller, 1992a). Experiments on the interaction between ChTx and the *Shaker* K^+ channel (F425G mutant) also suggest that Lys 27 interacts with K^+ ions on the *Shaker* K^+ channel pore (Goldstein and Miller, 1993). The lack of conservation in AgTxs of the functionally important residues for the ChTx-Ca^{2+}-activated K^+ channel interaction and ChTx-*Shaker* K^+ channel F425G interaction argues that the specific pair-wise interactions between toxin and channel residues on the interface are different in these toxins.

The number of amino acids between cysteine residues, except between the third and the four cysteines, is

conserved among the different toxin subclasses. Class I contains 10 amino acid residues between the third and fourth cysteines, class II, 11 residues and class III 9 residues. The differences in the number of amino acids in the segment between the third and fourth cysteines may be reflected in subtle (nonglobal) structural differences which can explain the functional differences between scorpion toxins. In the next chapter (chapter 3) the recently solved solution structure of AgTx2 is described and compared to other known scorpion toxin structures.

The feasibility of synthesizing recombinant AgTxs allows us genetically to manipulate the gene encoding AgTx for site directed mutagenesis studies. It also enables me to produce large amounts of purified toxin for structure determination purposes. These constitute the basis of our final goal of using these toxins as structural templates of the outer mouth of the ion conduction pathway on a cloned K^+ channel (chapters 4 and 5).

Chapter 3

STRUCTURE OF THE POTASSIUM CHANNEL INHIBITOR AGITOXIN2: CALIPERS FOR PROBING CHANNEL GEOMETRY

The capability of producing large amounts of purified toxin by recombinant methods, as described in chapter 2, allows to resolve its three-dimensional structure. Because of our current inability to obtain structural information from any K^+ channel by conventional protein structure determination methods, we intend to use AgTx2 as a probe for K^+ channel structure. The basic idea is simple (a full description is given in chapter 4); the known distance between residues on the toxin can be translated into the distance separating two residues in the channel, if the residues on the toxin interact closely with known residues on the channel.

The conservation of the six cysteine residues on the linear sequence of the scorpion toxins argues in favor of a common folding pattern (Garcia et al., 1994). The solved

solution structure of ChTx (Bontems et al., 1991b; Bontems et al., 1992), IbTx (Johnson and Snugg, 1992) and MgTx (Johnson et al., 1994) confirm this prediction. However, the structure of KTx has been recently solved (Fernandez et al., 1994) and shows differences when compared to the other toxin structures (see discussion section of this chapter). The common folding pattern of the K^+ channel inhibitors from scorpion venom consists of a triple-stranded antiparallel β-sheet and a single helix attached to the side of the β-sheet. Additionally, the structure is stabilized by three disulfide bonds.

The number of amino acids between the third and fourth cysteine residues is conserved amongst members of the same toxin subclass but is not conserved between different subclasses (see figure 2.7; Garcia et al., 1994). This suggests that toxins from different subclasses may differ slightly in their structures in the segment between the third and fourth cysteines. Consistent with this idea are studies showing that Arg24 of AgTx2, which lies in the segment between the third and fourth cysteines, is indispensable for conferring high affinity for the *Shaker*

K^+ channel (see chapter 4). Neutralization of this residue lowers the affinity by 1000-fold. The corresponding residue on the linear sequence of ChTx is a serine, but there is an arginine at position 25. Neutralization of Arg25 decreases the affinity of ChTx for the *Shaker* K^+ channel (F425G mutant) only by a factor of 14 (Goldstein et al., 1994). However, the same Arg25 is defined as a crucial residue for the binding of ChTx to a Ca^{2+}-activated K^+ channel (Park and Miller, 1992b; Stampe et al., 1994).

In this chapter the method used to synthesize isotopically labeled (C^{13}-N^{15}) AgTx2 for nuclear magnetic resonance (NMR) structure determination is described. The determination of the NMR structure of AgTx2 was done entirely in the laboratory of Dr. Gerhard Wagner by Dr. Andrzej Krezel and Dr. Chandrasekhar Khasibhatla with this labeled (C^{13}-N^{15}) AgTx2.

METHODS

Expression and purification of (C^{13}-N^{15}) AgTx2

The expression and purification of labeled AgTx2 was carried out essentially as described in chapter 2 with the following modification: *E.coli* harboring the AgTx1 plasmid were cultured in minimal medium containing in g/l: 12.8 $Na_2HPO_4 \cdot 7H_2O$, 3.0 KH_2PO_4, 0.5 NaCl, 1.0 $^{15}NH_4Cl$ (99%^{15}N, Isotec, Miamisburg, OH); in mM, 2.0 $MgSO_4$, 0.1 $CaCl_2$; and 0.2% ^{13}C-glucose (Isotec, Miamisburg, OH). The medium was supplemented with 0.1% of ^{13}C,^{15}N-celtone (Martek), a mixture of short ^{13}C,^{15}N-amino acids and peptides. The final yield was 0.7 mg of (C^{13}-N^{15}) AgTx2. Trypsin was used to cleave the toxin from the fusion protein.

The expression vector was slightly different from the original one (figure 2.3) in the recognition site for peptidase. To improve toxin yield the factor Xa protease recognition site (recognizing the amino-acid sequence IEGR) was used in place of our original enteropeptidase recognition site. The factor Xa recognition site was generated by PCR mutagenesis with a single mutant

oligonucleotide (30 bases in length) coding for the factor Xa recognition site, which covered the Sal I restriction site up to the third codon of the toxin DNA sequence. Ultimately, trypsin was chosen for proteolytic cleavage over factor Xa because of its better yield and lower cost. Trypsin cleaves at the carboxyl side of arginine and lysine residues. The cleavage reaction was performed by adding 5 μg of trypsin per mg of fusion protein along with 100 mM NaCl and 1 mM $CaCl_2$, final concentrations. The integrity of AgTx2 after trypsin cleavage was demonstrated by HPLC of a reduced and carboxymethylated form of purified AgTx2. Further verification was done by mass spectrometry and amino acid analysis.

RESULTS

Secondary structure

AgTx2 is a highly structured peptide. Most of its linear sequence is involved in the formation of secondary structure, a triple stranded antiparallel β-sheet and a single helix (figure 3.1). The three strands of the β-sheet, S1, S2 and S3 are formed by residues residues 2 to 8, 24 to 29, and 32 to 36, respectively. The two outer strands of the β-sheet, S1 and S2, are connected by the helix. S3 is in the center of S1 and S2. The helix starts at residue 11 and finishes at residue 22. From residues 11 to 15 the helix adopts a 3_{10}-helix configuration then to continues as an α-helix.

Tertiary structure

AgTx2 has an asymmetric shape that resembles an ellipse, with a long axis of about 30 Å and two short axes of about 20 Å (figure 3.2). AgTx2 appears to be a "tightly packaged" product of three disulfide bonds, two of which bring together the β-sheet and the helix. Most of the amino

acid residues are exposed to solvent, except for the six cysteines, Gly26 and the side chain of Met23, which form the core of the molecule (figure 3.2).

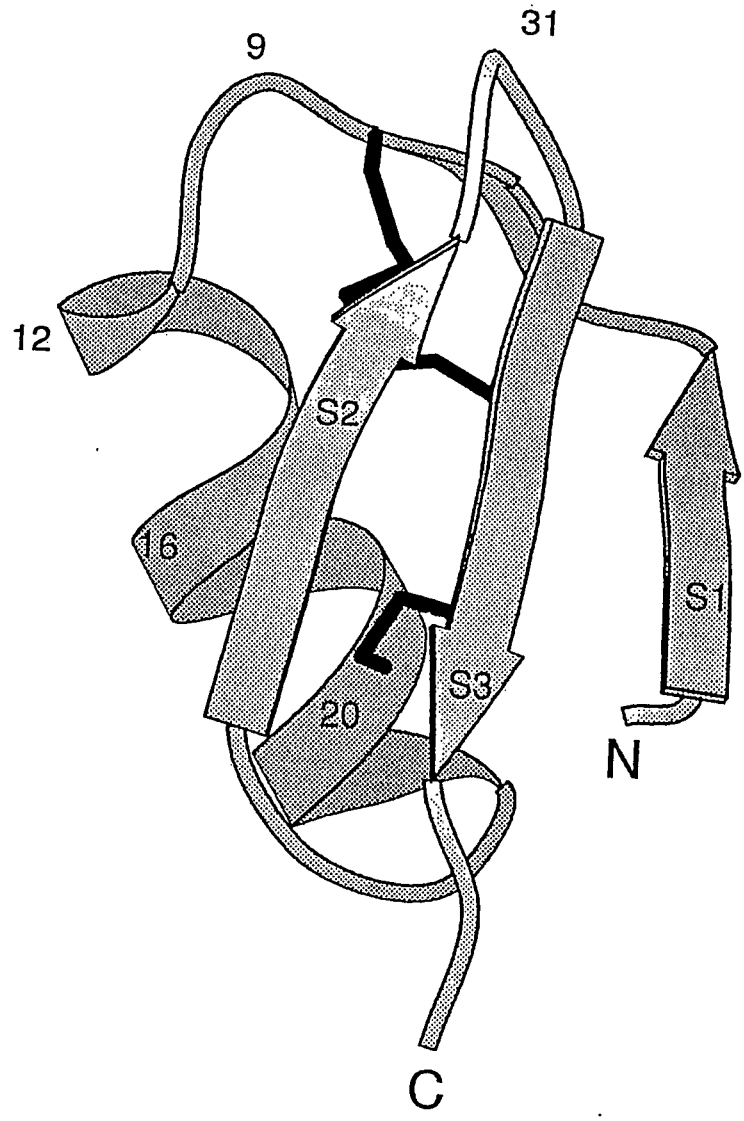

Figure 3.1. Diagram of the secondary structure of AgTx2. The three strands of the antiparallel β-sheet, S1, S2, and S3 consist of the residues 2 to 8, 24 to 29, and 32 to 36, respectively. The helix starts as a 3_{10}-helix (residues 11 to 14) and continues as an α-helix (residues 15 to 22). The dark lines correspond to the three disulfide bonds; taken from (Krezel et al., 1995)).

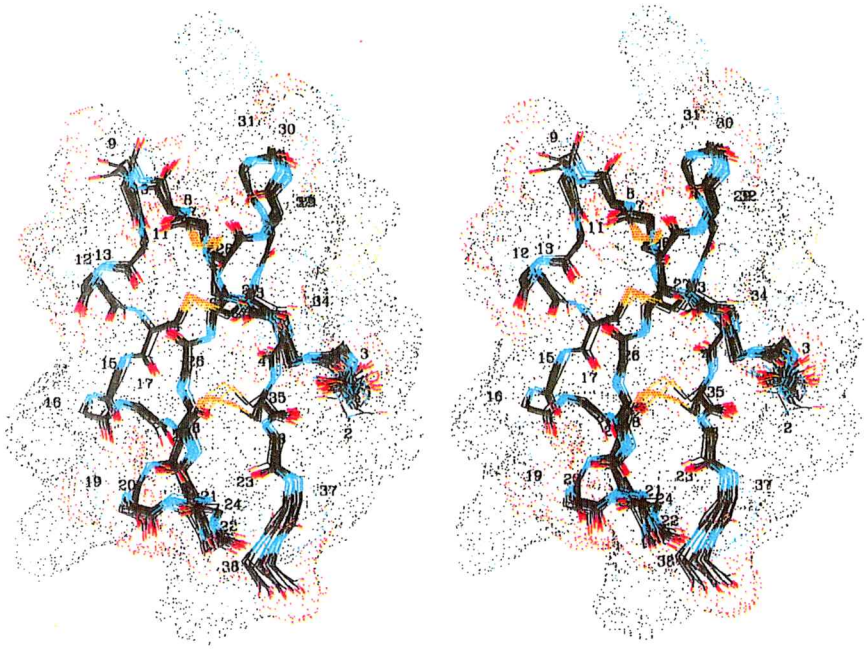

Figure 3.2. Three-dimensional structure of AgTx2. The diagram shows a stereo view of the backbone for 17 calculated structures of AgTx2 and the van der Waals surface for one structure. All heavy atoms are shown: carbon in black, nitrogen in blue, oxygen in red, and sulfur in yellow. Two disulfide bonds connect the helix with the central strand of the β-sheet. The root-mean-square deviation of atomic coordinates for the average backbone (residues 3 to 36) is 0.37 Å (taken from Krezel et al., 1995).

DISCUSSION

The solved structure of AgTx2 is very well defined as reflected in the low value of the root-mean-square for the backbone atomic coordinates (0.37 Å for residues 3 to 36) of the 17 calculated structures (Krezel et al., 1995). AgTx2 is an extremely rigid peptide. The rigidity of AgTx2 makes it suitable for site directed mutagenesis. Substitutions of amino acid residues, that are exposed to the solvent, in AgTx2 are unlikely to alter the overall structure. This is an important feature for using AgTx2 as a structural probe of the *Shaker* K^+ channel

The three-dimensional structure of AgTx2 closely resembles the structure of other known K^+ channel inhibitors isolated from scorpion venom, such as ChTx (Bontems et al., 1991b; Bontems et al., 1992), IbTx (Johnson and Snugg, 1992) and MgTx (Johnson et al., 1994). The structure of these toxins, determined by NMR, have essentially the same folding. However, the structure of Ktx (Fernandez et al., 1994), solved recently by NMR, differs from this common folding pattern in the orientation of the

amino-terminal strand of the triple stranded antiparallel β-sheet. This difference is not very likely because of the similarity of the structure between the known K^+ channel inhibitors isolated from scorpion venom which structures had been determined based on a larger number of structural constrains. Additionally the amino-acid sequence of KTx differs from that of AgTx2 in only four residues (see figure 2.7).

The structural motif displayed by these toxins, a triple stranded antiparallel β-sheet and a helix attached to one side, seems to be a common motif among peptide inhibitors of ion channels (Bontems et al., 1991a). Figure 3.3A shows the superimposition of the backbones of AgTx2, ChTx and two others peptide inhibitors from scorpion. The backbone of AgTx2 superimposes well with that of ChTx. One major structural difference occurs in the loop connecting the carboxy-terminal end of the α-helix with the β-sheet (Krezel et al., 1995). This loop is formed by residues lying in the segment between the third and fourth cysteines. The alignment of AgTx2 and ChTx sequences based

A.

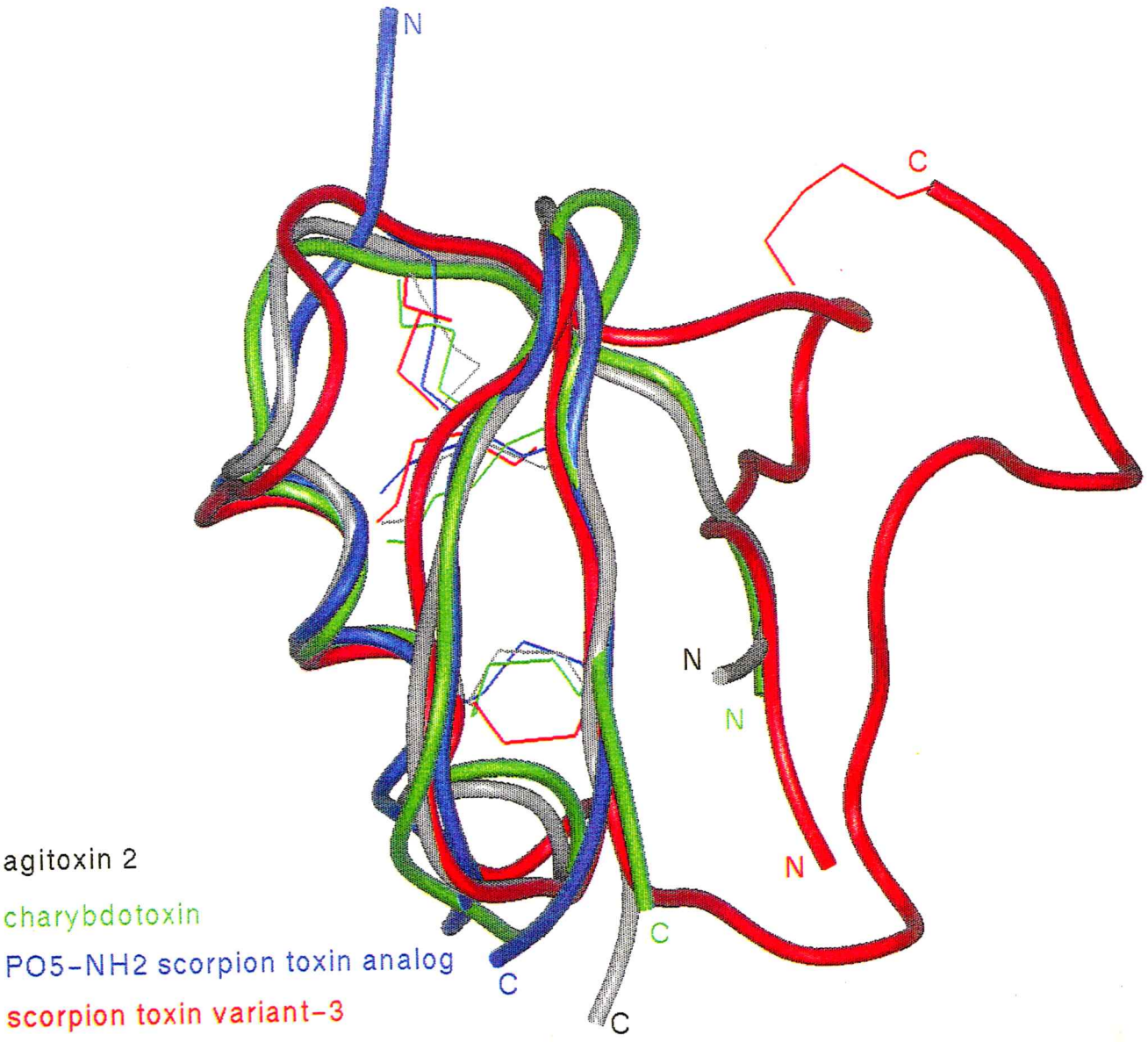

Figure 3.3 A. Superimposition of AgTx2 and ChTx structures. Diagram of superimposed backbone structures of scorpion toxins. The amino and carboxy termini are indicated. AgTx2 is shown in black and ChTx in green. The motif consisting of a triple stranded antiparallel β-sheet linked to a short helix seems to be the common pattern for all the scorpion toxins. The backbone of two other toxins, scorpion toxin variant-3 (shown in red, known to block voltage-activated Na^+ channels) and PO5-NH_2 (shown in blue, an analog to leiurotoxin I, known to block a low-conductance Ca^{2+}-activated K^+ channel) are included (kindly provided by Krezel and MacKinnon).

B.

	3th	4th
AgTx2	GVPINVSCTGSPQCIKPCKDAG-MRFGKCMNRKCHCTPK	
ChTx	ZFTNVSCTTSKECWSVCQRLHNTSRGKCMNKKCRCYS	

Figure 3.3 B. Amino-acid sequence alignment of AgTx2 and ChTx based on the solved structures. The sequence alignment was based on the spatial correspondence of the N,C^{a},C' backbone atoms of both structures. The third and fourth cysteine residues are numbered above the AgTx2 amino acid sequence. Between the third and fourth cysteine residues a gap is introduced in the AgTx2 sequence (marked with a dash) and AgTx2 contains fewer bulky residues in that region. The functionally important residue Arg24 of AgTx2 is underlined.

on the spatial correspondence of the amino-acid residues (figure 3.3B) introduces a gap in the AgTx2 sequence and also

AgTx2 has amino acid residues with small side chains (Ala21 and Gly22) relative to the ones in ChTx in the corresponding positions in that loop.

It has been shown that Arg24 of AgTx2 is crucial for the high affinity binding of AgTx2 to the *Shaker* K^{+} channel (chapter 4). Arg24, located in between the third and fourth cysteine residues, interacts with the side chain of Phe25 on AgTx2, resulting in restricted mobility of the former (figure 3.4). As a consequence of this interaction, Arg24

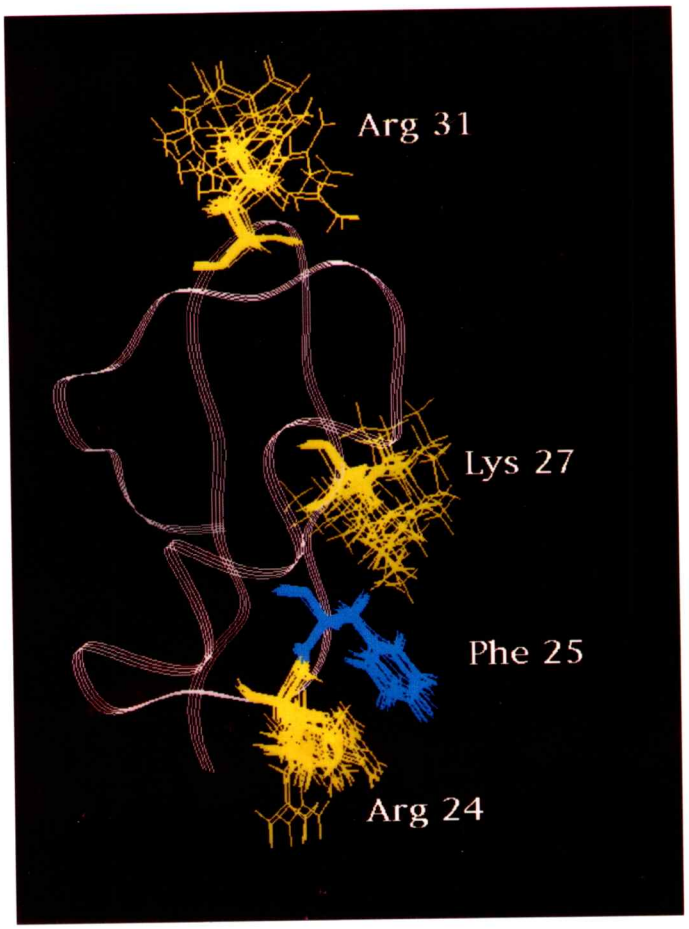

Figure 3.4. Arginine 24 of AgTx2 is well defined in space. Average ribbon diagram representing an average backbone structure and three side chains for 17 AgTx2 calculated structures is shown. The positions of the different rotomers of Arg24 are very restricted in space as a result of the interaction with the side chain of Phe 25.

is strongly constrained in space.

The solved structure of AgTx2 has begun to provide the structural basis for the specificity of AgTx2 for the *Shaker* K^+ channel. The known toxin dimensions, as well as further studies on the AgTx2-*Shaker* K^+ channel interaction, will give us a better picture of what the toxin binding site looks like

Chapter 4

REVEALING THE ARCHITECTURE OF A K^+ CHANNEL PORE THROUGH MUTANT CYCLES WITH A PEPTIDE INHIBITOR.

The knowledge of the structure of AgTx2 (chapter 3 and Krezel et al., 1995) makes possible the use of this toxin to obtain structural information about the pore forming region of the *Shaker* K^+ channel. The toxin could act as a relative coordinate system to determine the spatial distribution of channel residues forming the binding site.

Thermodynamic double mutant cycles have provided a formalism for studying energetic coupling between amino acids on the same polypeptide chain (Carter et al., 1984; Serrano et al., 1990; Horovitz and Fersht, 1990). A systematic analysis using thermodynamic double mutant cycles was developed in order to identify pair-wise interactions between amino acid residues on AgTx2 and the *Shaker* K^+ channel and AgTx2. The identified channel

residues are organize in the space with respect to the AgTx2 structure.

In this chapter the thermodynamic double mutant cycles approach with AgTx2 and the *Shaker* K^+ channel is described.

METHODS

Mutagenesis and expression of AgTx2 and *Shaker* K^+ channel.

All experiments were carried out using an inactivation-removed *Shaker* K^+ channel clone expressed in Xenopus oocytes (Hoshi et al., 1990). Oocytes were prepared and injected with in vitro transcribed RNA as described in methods section, chapter 2. Channel mutants clones were available in the laboratory and were produced by complementary strand synthesis (Kunkel, 1985). Recombinant toxin was prepared as described in methods section, chapter 2, with the following modifications. Trypsin was used to cleave the toxin from the fusion protein (5 µg of trypsin per mg of fusion protein and 100 mM NaCl, 1mM $CaCl_2$, final concentrations were added to the cleaving reaction). The last step of toxin purification performed by reverse-phase HPLC using a C_8-column was slightly modified by using a linear gradient 0 to 50% acetonitrile in 30 minutes. An extinction coefficient of 8.6 mM^{-1} cm^{-1} at 235 nm was used to calculate toxin concentration. Mutants were produced in the toxin gene using PCR mutagenesis with a mutant

oligonucleotide. Two overlapping mutant oligonucleotides (15 bases) were chemically synthesized in an Applied Biosystems DNA synthesizer model 391. Two independent PCR reactions with each mutant oligonucleotide were performed. The PCR products were gel purified from a 2% agarose gel and used as primers for a second PCR along with the flanking primers #2 and #4 (see figure 2.2). The PCR product was phenol extracted, ethanol precipitated, digested with Sal I and Hind III, gel purified, and ligated to the vector. The mutant clones were confirmed by dideoxy DNA sequencing across a Sal I-Hind III cassette containing the coding sequence.

Electrophysiological recording.

K^+ currents were recorded with a two-electrode voltage clamp amplifier (Warner Instruments). Recording solution contained in millimolar: 95 NaCl, 2 KCl, 0.3 $CaCl_2$, 1 $MgCl_2$, 5 HEPES buffer, pH 7.6. Currents were elicited with a 50 ms step to 0 mV every 5 to 25 sec from a holding potential of -80 mV. Perfusion with toxin-free and toxin-containing solution was controlled with separate lines

using computer-driven solenoids valves. Bovine serum albumin at a concentration of 50 μg/ml was used to prevent non-specific adherence of toxin to the perfusion lines. Current magnitudes ranged from 0.5 to 1.5 μA. The time course of blockade was monitored to ensure that equilibrium inhibition was achieved and to confirm that the control current level was the same before addition and after removal of toxin. From 3 to 8 experiments were made on separate oocytes. The equilibrium inhibition constant (Ki) was calculated according to $Ki = [T](I/I_0)/(1-(I/I_0))$ where I_0 is the control current level and I is the current in the presence of toxin concentration [T].

RESULTS

We intend to organize in space residues on the S5-S6 linker of the *Shaker* K^+ channel (figure 4.1A), known to be the main determinant of the scorpion toxin binding site, with respect to the AgTx2 structure (figure 4.1B). To organize channel residues in space with respect to the AgTx2 structure, specific pairwise interactions between residues on the toxin and on the channel must be identified. Point mutations of several charged residues in the S5-S6 linker of the *Shaker* K^+ channel alter toxin inhibition by an electrostatic mechanism (MacKinnon and Miller, 1989a; MacKinnon et al., 1990). I exploited the known electrostatic component of the toxin-channel interaction and thus focused on acidic or basic residues (figure 4.1A and B). To identify pairwise interactions between amino-acid residues on the toxin and on the channel two residues, one on the toxin and one on the channel, were mutated. The cross influence of one mutation on the effect of another can be quantified using a thermodynamic double mutant cycle (figure 4.1C). A detailed description of mutant cycles applied to interactions between amino acids

A.

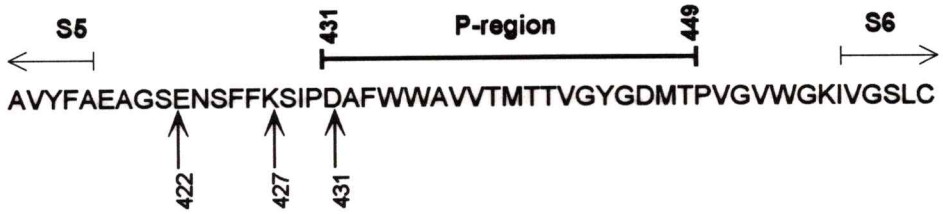

B.

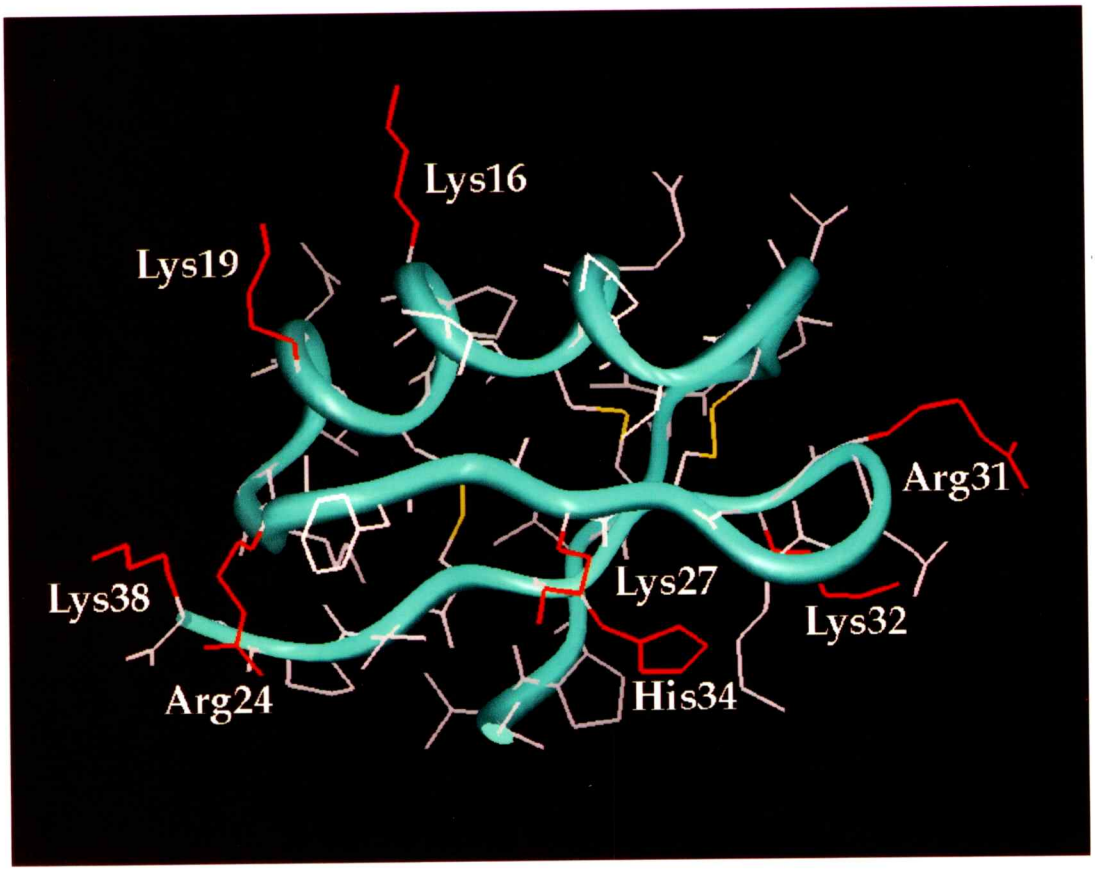

Figure 4.1 (A and B). Thermodynamic mutant cycles identify interactions between amino acids on the *Shaker* K^+ channel and AgTx2. **A.** The partial sequence of a *Shaker* K^+ channel subunit shows the S5-S6 linker and indicates the three toxin-interacting residues under study (arrows). The P-region extends from residue 431 to 449. **B.** AgTx2 structure without the hydrogen atoms is shown with a blue backbone ribbon. The eight basic amino acids studied are shown in red and the three disulfide bridges in yellow.

C.

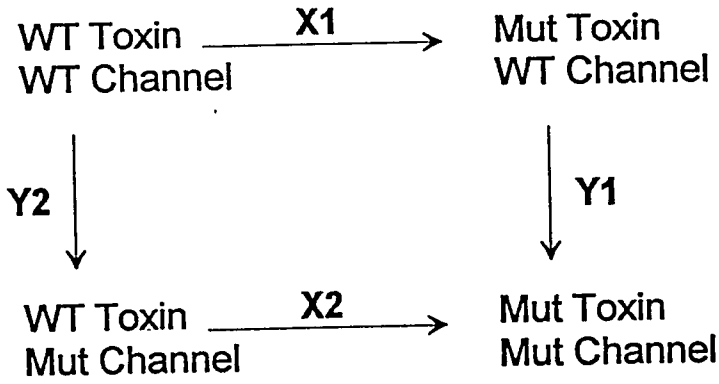

D.

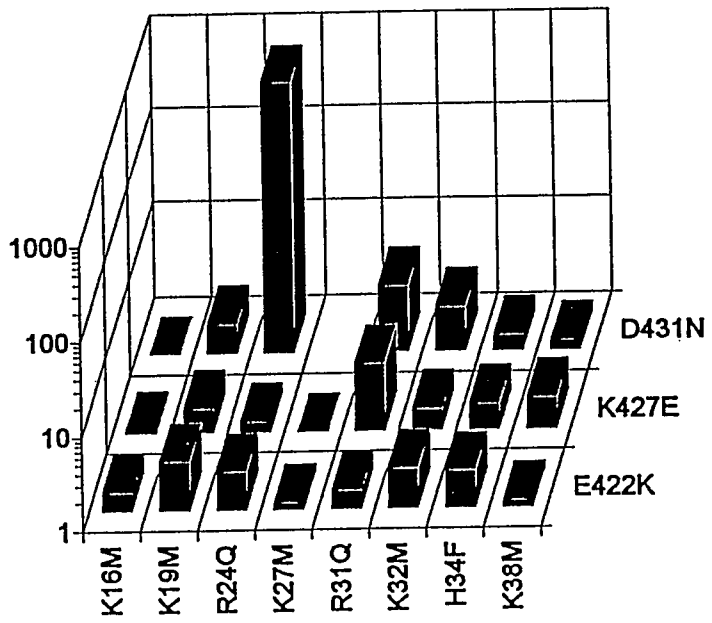

Figure 4.1. (C and D). C. Equilibrium inhibition constants for the affinity of wild type toxin (WT Tox) and mutant toxin (Mut Tox) for a wild type channel (WT Chan) and mutant channel (Mut Chan) define a thermodynamic cycle where X1, X2, Y1 and Y2 represent fold change in affinity along the arrow (inhibition constant at the tail of the arrow divided by that at the head). D. The Ω plot graphs Ω values calculated according to Eq. 2 for the paired mutations shown in single letter code. Our inability to determine Ω for the K27M/D431N pair is compatible with their independence (see table 4.1).

within a single protein has been given (Carter et al., 1984; Serrano et al., 1990; Horovitz and Fersht, 1990). For each cycle (see figure 4.1C), the pair of amino acids under study, one on the toxin and one on the channel are both mutated. Each corner of the cycle corresponds to the inhibition equilibrium constants for the four toxin-channel pair, (wild-type toxin/wild-type channel; mutant toxin/wild-type channel; wild-type toxin/mutant channel and mutant toxin/mutant channel). The horizontal arrows connecting a given toxin-channel pair indicate mutation of the toxin and the vertical arrows indicate mutation of the channel. The effect of the toxin mutation on the affinity for the wild-type channel is reported as X1 (top horizontal bar). Then the effect on affinity of the same toxin mutation is tested against a channel with a point mutation and reported as X2 (bottom horizontal arrow). The number assigned to each arrow corresponds to the factor by which affinity changes along the direction of the arrow (i.e. X1 = Ki(wt:wt)/Ki(mut:wt), where Ki(toxin:channel) refers to the equilibrium inhibition constant for the indicated pair. Because the overall affinity change in going from the wild-

type toxin / wild-type channel interaction (upper left) to the mutant toxin / mutant channel interaction (lower right) must be the same regardless of the pathway taken the following thermodynamic relationship is fulfilled

$$X1 \cdot Y1 = X2 \cdot Y2. \qquad (1)$$

Dividing both sides of Eq. 1 by X2·Y1 leads to the coupling coefficient, Ω, defined as

$$\Omega = \frac{X1}{X2} = \frac{Y2}{Y1} = \frac{Ki(wt:wt) \cdot Ki(mut:mut)}{Ki(wt:mut) \cdot Ki(mut:wt)} \qquad (2)$$

Because Ω is a ratio of a ratio of equilibrium constants it is related to the difference in the difference in free energy change brought about by the mutation on the toxin and on the channel. Thus, in energetic terms, it reports the degree of interaction, or coupling energy brought about by the double mutation.

The value of Ω reflects whether or not two residues interact. Consider two cases; first, the mutated residues,

one on the toxin and one on the channel do not interact and, second, the mutated residues do interact. The outcome for these two cases is radically different. In the first case (mutated residues do not interact) the mutation of the toxin is not "sensed" by the mutation of the channel; therefore, the toxin mutation alters the affinity by the same factor for both the wild type and the mutant channel (i.e. X1 = X2). Thus, if the two mutated residues are independent of one another Ω will be unity. In the second case (mutated residues interact) the toxin mutation has a given effect on the affinity for the wild-type channel. Because the mutated residue on the toxin interacts with that on the channel, there is a different effect on the affinity for the mutant channel, which depends on the amino acid residue at that particular position on the channel (i.e. X1 $\neq$ X2). Thus if the residues interact and the mutations alter their interaction Ω will deviate from unity. It is possible, but unlikely, for mutations to alter an interaction between two residues in such a way that there is energetic compensation giving rise to an Ω value of unity. To allow easy comparison of magnitudes,

throughout this study Ω is reported as a number greater than unity (if Ω is less than unity according to Eq. 2 then its reciprocal is given.).

An Ω plot for charge-neutralizing mutations of the eight basic residues on the toxin (figure 4.1B) with charge-altering mutations at positions 422, 427, and 431 on the channel (figure 4.1A) is shown in figure 4.1D, Table 4.1). Ω for the pair R24Q (toxin) / D431N (channel) stands out above the others. Its large Ω value results from the R24Q mutation reducing toxin affinity for the wild type channel about 1000-fold (X1 = 977.03), but having little effect on toxin binding to a D431N mutant channel (X2 = 1.33) (Table 4.1). From the Ω definition this outcome is expected if Arg24 and Asp431 form a strong and specific interaction with each other. The magnitude of Ω for the R24Q/D431N pair corresponds to a coupling energy of about 4kcal $mole^{-1}$. Mutation of either residue alone disrupts the interaction so that subsequent mutation of the second residue has little further effect. This result contrasts with the independence of mutations observed for many other pairs. For example, the K427E channel mutation and the R24Q

toxin mutation both have very large effects on affinity, but Ω for this pair is near unity (Table 4.1, figure 4.1).

	WT (nM)	E422K (nM)	Ω	K427E (nM)	Ω	D431N (nM)	Ω
WT	0.74 ± 0.04	9.1 ± 0.7		0.007±0.001		2233 ± 60	
K16M	1.42 ± 0.03	11.1 ± 0.8	1.6 ± 0.2	0.015±0.001	1.1 ± 0.2	4092 ± 302	1 ± 0.1
K19M	2.7 ± 0.2	9.9 ± 0.5	3.4 ± 0.4	0.014±0.001	1.8 ± 0.3	3791 ± 107	2.1 ± 0.2
R24Q	723 ± 43	3486 ± 264	2.6 ± 0.3	9.0 ± 0.7	1.3 ± 0.2	2976 ± 396	733 ± 116
K27M	575 ± 42	8400 ± 1000	1.2 ± 0.2	5.4 ± 0.2	1.0 ± 0.2	NB	....
R31Q	4.3 ± 0.3	32.7 ± 1.7	1.6 ± 0.2	0.21 ± 0.01	5.2 ± 0.9	2619 ± 213	5.0 ± 0.6
K32M	4.4 ± 0.3	20.0 ± 0.7	2.7 ± 0.2	0.025 ± 0.003	1.7 ± 0.3	4522 ± 223	3.0 ± 0.3
H34F	0.8 ± 0.1	24.9 ± 0.3	2.5 ± 0.5	0.004±0.001	1.9 ± 0.6	3724 ± 174	1.5 ± 0.3
K38M	0.91 ± 0.03	9.1 ± 1.0	1.2 ± 0.2	0.019±0.001	2.2 ± 0.3	2084 ± 160	1.3 ± 0.1

Table 4.1. Inhibition constants and Ω values for channel and toxin mutants are tabulated. The toxin mutations (left) were designed to neutralize basic amino acids. The channel mutations (top) altered the charge at three positions (422, 427 and 431) in the S5-S6 linker. Each Ki (nM) for the toxin and channel shown was measured as described in methods and is the mean ± SEM of 3 to 8 separate measurements. NB refers to no inhibition at 2 μM. (If the K27M and D431N mutations are independent then the expected Ki for this pair is 1.7 mM.) Ω was calculated according to Eq. 2 but is reported as a number greater than unity (see text).

Inspection of the Ω plot leads to the conclusion that the strong coupling between these two mutated residues must come about through their local interaction and not through a global structural change of either the toxin or the

channel. For example, if the R24Q mutation altered the toxin structure, or caused the toxin to change its position in the binding site, then R24Q would in general be strongly coupled to many other channel mutations. Likewise, if the D431N mutation produced a global alteration of the channel structure then strong coupling to multiple toxin mutations would be expected. Therefore, the singular large Ω value at R24Q/D431N along the toxin and channel dimensions of the plot provides internal support for the structural integrity of both mutated molecules and reinforces the conclusion that Asp431 interacts locally with Arg24.

Another, smaller but significant Ω is observed with the same Asp431 channel residue and Arg31 on the toxin. This does not contradict the above statement if we remember that the *Shaker* K^+ channel is formed by the assembly of four identical subunits; therefore the channel exposes four Asp431 to the toxin. Thus, the fact that two toxin residues spatially separated from each other (25 Å apart) interact with the same channel residue is understood on the basis of the channel geometry. The interaction between Arg31 and Asp431 can be predicted by considering both the four-fold

symmetry of the *Shaker* K^+ channel (MacKinnon, 1991) and the toxin's dimensions, as described below. Previous biophysical studies demonstrated that Lys27 on ChTx interacts with K^+ ions inside the Ca^{2+}-activated K^+ channel pore (Park and Miller, 1992a; MacKinnon and Miller, 1988). Studies on the interaction between ChTx and the *Shaker* K^+ channel with the F425G mutation that confers sensitivity to ChTx suggest that Lys27 is also located over the pore (Goldstein and Miller, 1993). Besides the six cysteine residues, Lys27 is the only fully conserved residue among the K^+ channel inhibitors from scorpion venom (Garcia et al., 1994). If Lys 27 on AgTx2 is located centrally over the pore, then the strong interaction between Arg24 and Asp431 predicts that Arg31, located at the opposite side of the toxin from Arg24 (figure 4.2), should also interact with the Asp431 residue located in the diagonally-opposed channel subunit.

Arg31 and Arg24 are not exactly symmetric with respect to Lys27 and, therefore, their interactions with Asp431 residues on diagonal subunits should not be identical. Nevertheless, the strong interaction, which so tightly

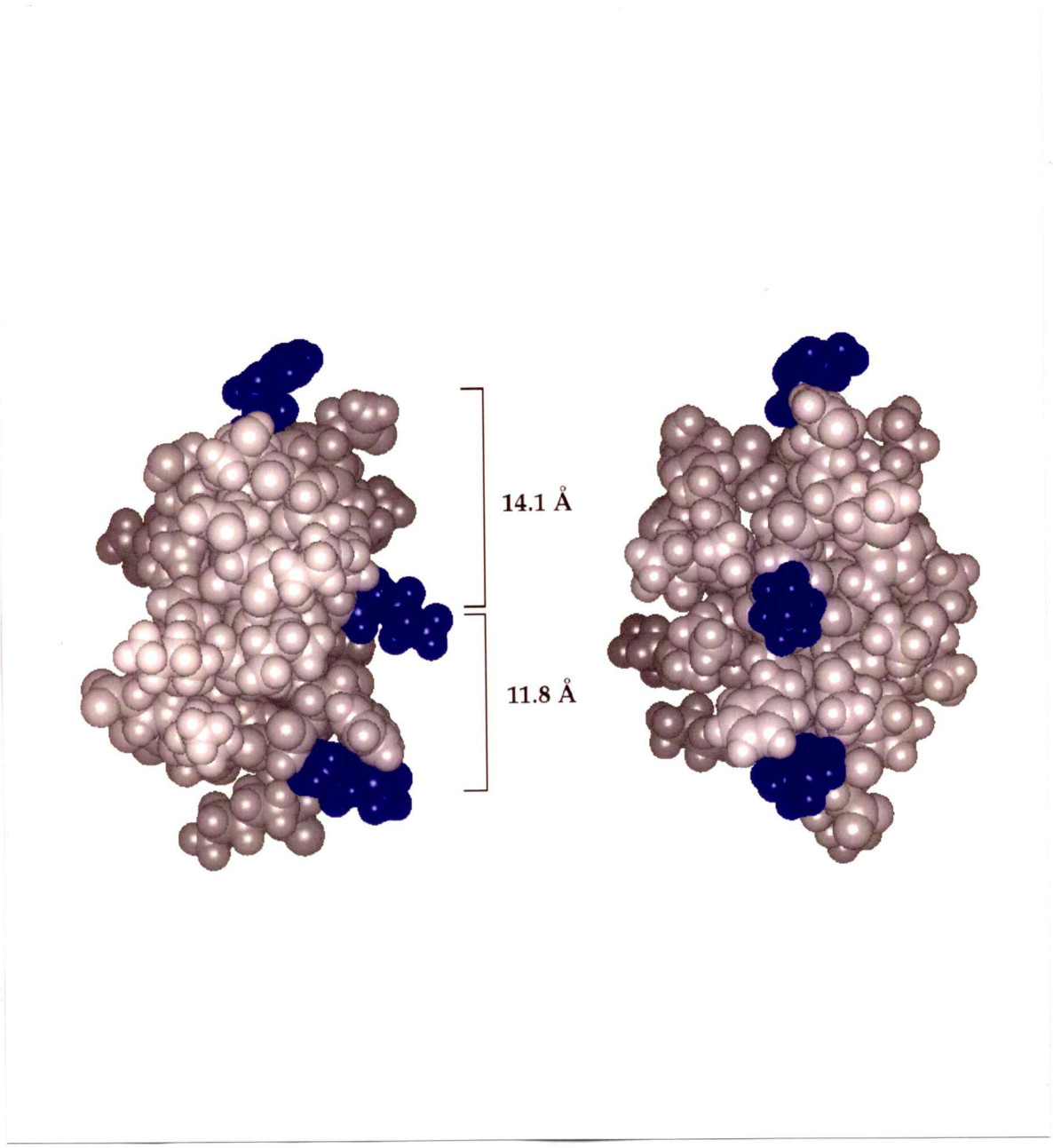

Figure 4.2. A CPK model of AgTx2 shows (in dark) the side chains of Arg24 (bottom), Lys27 (middle) and Arg31 (top). The distances between the γ-carbons of Arg24 and Lys27 and Arg31 and Lys27 are indicated. Right panel is a 90° rotation of the molecule shown in the right panel.

constrains the location of Asp431 on one subunit with respect to Arg24, would place Asp431 on the diagonal subunit within a few angstroms of Arg31; thus a through-space electrostatic interaction is likely to occur between them. The Ω value for the R31Q/D431N pair, 5 ± 0.6 (figure 4.1D; Table 4.1), corresponds to a coupling energy of approximately 1 Kcal $mole^{-1}$, which is around the magnitude expected for through-space electrostatic coupling. For example, using Debye-Hückel theory, 1 Kcal $mole^{-1}$ translates into a 3 Å separation between two unit charges in a 100 mM NaCl solution. In addition, the fact that many Ω values are close to unity in the Ω plot reflects a rapid decay of the electric potentials across space and therefore supports the proposal that Asp431 and Arg31 must be close in space.

Further to test an electrostatic mechanism between residues 31 on the toxin and 431 on the channel, a network of cycles was constructed by making multiple amino acid substitutions at both positions (figure 4.3). The Arg31 was substituted with Lys (R31K), to preserve the positive charge in that position, or by a Gln (R31Q), to neutralize

the charge. Asp431 was substituted by Glu (D431E, to preserve charge) or an Asn (D431N, to neutralize the charge). The combination of three different residues at position 31 (Arg, Lys, Gln) on the toxin and three different residues at 431 (Asp,Glu,Asn) on the channel give rise to nine possible thermodynamic cycles for which the Ω value was calculated (figure 4.3, bottom panel). A through-space electrostatic mechanism predicts that mutations will show coupling (i.e. Ω deviate from unity) only if charge is altered on both the toxin and the channel. If charge is conserved at the mutated site on either or both proteins then the electrostatic interaction is not altered and, therefore, no coupling should be observed (Ω = 1). The pattern of Ω values, larger only for cycles where charge perturbation occurs on both the toxin and the channel (cycles shown in bold) fulfills the above prediction. These results firmly establish the electrostatic nature of the interaction between residues 31 (toxin) and 431 (channel). We, therefore, conclude that these residues are within a few angstroms of each other, as was hypothesized based on the previously mentioned geometric considerations.

Figure 4.4 shows the cycle network analysis to characterize the strong interaction between Arg 24 on the toxin and Asp431 on the channel. The same substitutions as for the 31/431 pair were made: Arg24 on the toxin was substituted with Lys and Gln and Asp431 on the channel was substituted with Glu and Asn. In contrast to the pattern observed for the 31/431 pair, the 24/431 pair shows large Ω values for all cycles independent of the charge perturbation (figure 4.4, bottom panel). Therefore the chemical nature rather than the charge is important for the interaction between Arg24 and Asp431. These results confirm the idea that these residues interact through shorter range molecular forces rather than through-space electrostatics. Arg24 and Asp431 apparently come into intimate contact either sterically (with an electrostatic component) or, more likely, through the formation of an ionized hydrogen bond (salt bridge). The side chain of arginine residues can serve as hydrogen-bond donors while the side chain of aspartate residues serves as hydrogen-bond acceptors (Branden and Tooze, 1991).

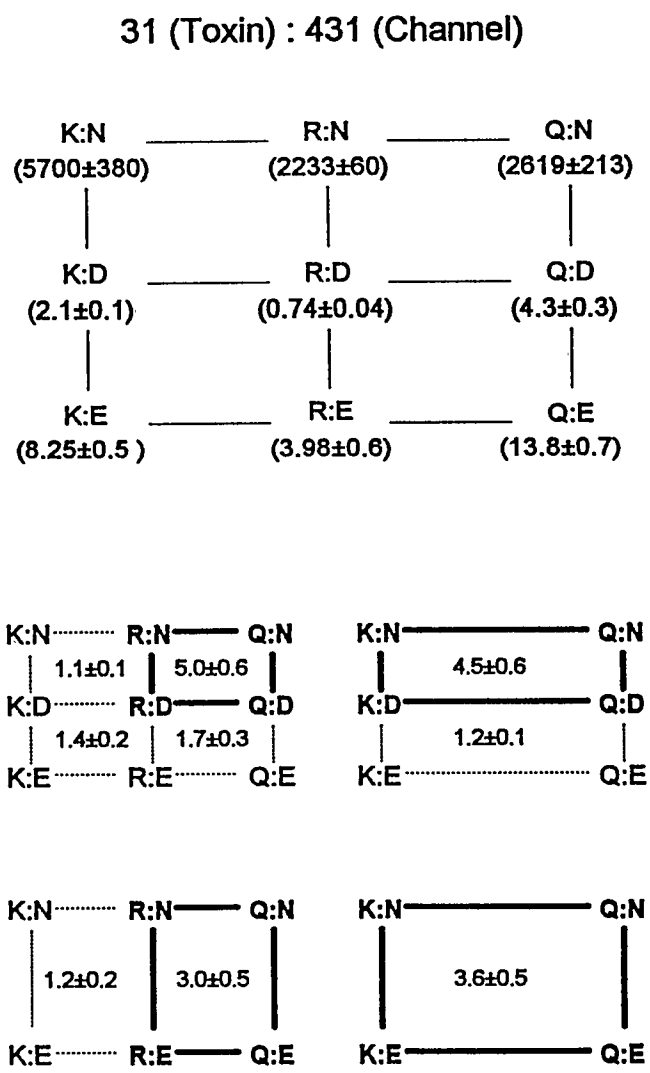

Figure 4.3. Multiple amino acid substitutions involving a pair of residues allow the construction of a cycle network for studying the interaction between mutated residues. The network contains nine toxin-channel pairs corresponding to all combinations of three residues at position 31 (toxin) with three residues at position 431 (channel). At each node, the amino acid (single letter code) on the left refers to the toxin residue and that on the right refers to the channel residue. Inhibition constants (nM, mean ± SEM of 3 to 8 measurements) for each toxin-channel pair are shown in parenthesis (top panel). The value of Ω for every possible cycle defined by the network is shown (bottom panel). Ω for each cycle (reported as a number greater than unity) was calculated according to Eq. 2 using Ki values corresponding to the interaction pairs at the four corners of the cycle. Cycles with larger Ω values (3 to 5) are shown in bold. Note that Ω for the four smallest cycles fully determine Ω for the remaining five larger cycles.

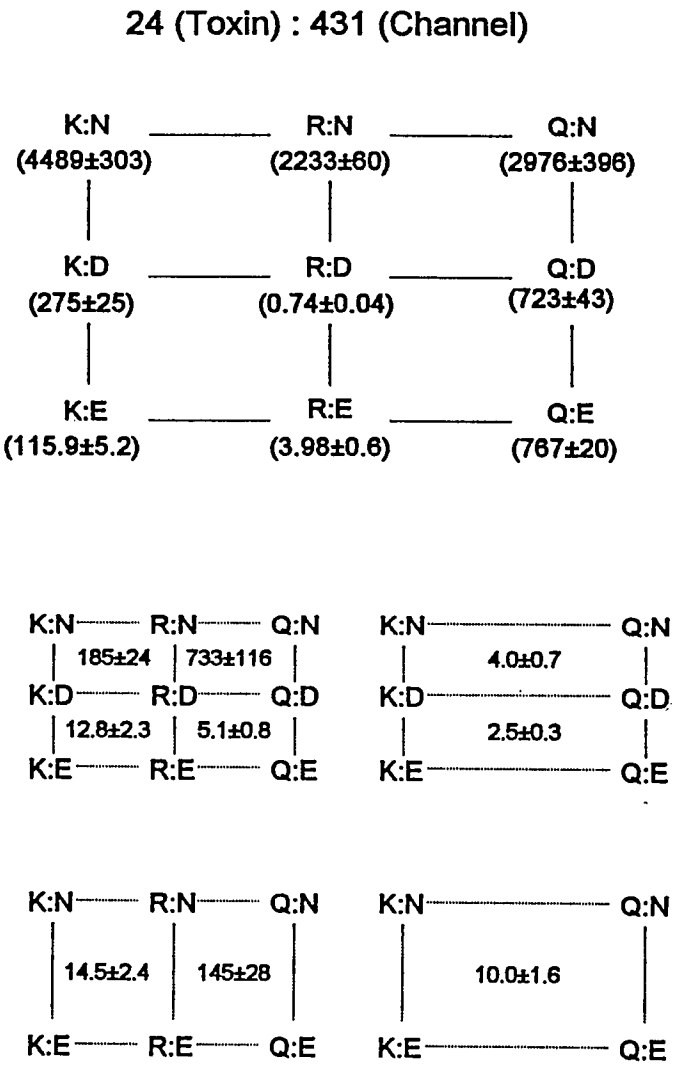

Figure 4.4. Network cycle analysis for studying the interaction between mutated residues at position 24 (toxin) and 431 (channel). All the Ω values are large independent of charge perturbation. See legend figure 4.3 for description.

DISCUSSION

Thermodynamic double mutant cycles were applied to reveal pairwise interactions between the eight basic residues of AgTx2 and three channel residues in the S5-S6 linker of the *Shaker* K^+ channnel. A coupling coefficient, Ω, was defined that reflects the degree of interaction between two residues, one on the toxin and one on the channel, brought about by mutation of both residues. Two Arg residues on the toxin, at position 24 and 31, were found to interact with the same Asp431 channel residue. Further application of thermodynamic double mutant cycles were used to identify the nature of the interaction between residues through cycle a network analysis. It was found that Arg24 interacts strongly through short range molecular forces and Arg31 via a through-space electrostatic mechanism. Therefore, Arg24 and Arg31 are close in space to Asp431 on the channel. Because the channel has four-fold symmetry and because the distance separating these two arginine residues in the toxin is about 25 Å, Arg24 and Arg31 must interact with aspartate 431 residues on

diagonally-opposed channel subunits. The physical proximity of Arg24 and Arg31 to their respective Asp431 residues allows us to translate the distance separating these two arginine residues on the toxin into the distance separating two Asp431 residues on diagonally-opposed channel subunits.

The relationship between the Asp431 residues on four channel subunits with respect to the toxin is shown in figure 4.5. Asp431, corresponding to the amino-terminal limit of the P-region, is located 12 to 15 Å away from the central axis. The range is derived from the range in the distance separating Arg24 and Arg31 determined by measuring the distance between the guanidinium carbons in different rotomers of a set of 17 calculated AgTx2 structures. The distance of closest approach was 24 Å and of greatest separation was 31 Å.

The distance (12 to 15 Å) is nearly ten times greater than the radius of a K^+ channel selectivity filter, estimated by functional measurements to be about 1.5 Å (Hille, 1975). The surprisingly distant radial location of Asp431 raises the possibility that a significant segment of the P-region could be oriented parallel rather than

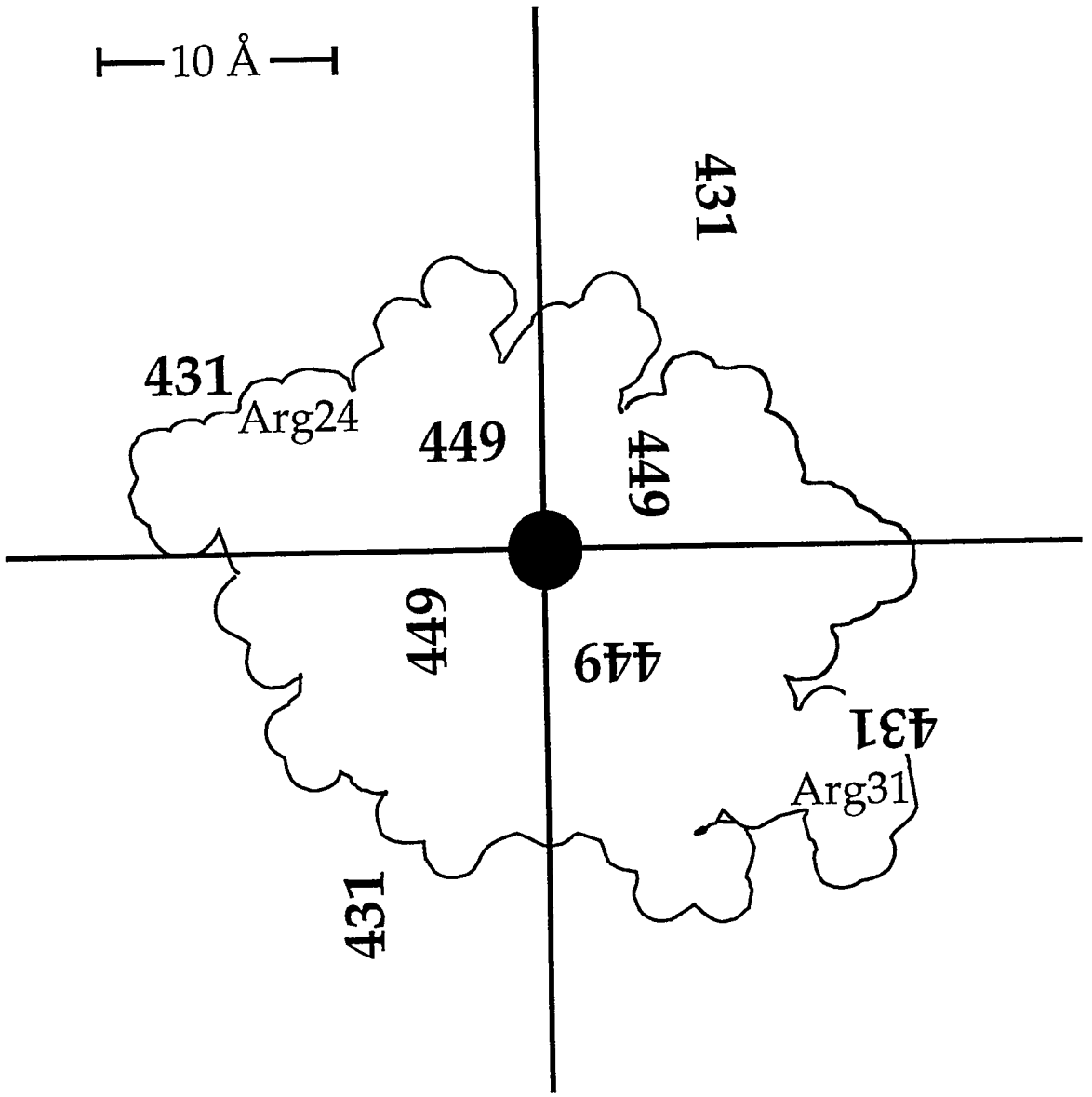

Figure 4.5. Channel residue Asp431 is between 12 and 15 Å from the central axis of the K^+ channel pore. The scalloped outline shows the shadow of AgTx2, oriented with Lys27 over the pore (black circle) at the interface between four subunits (defined by axes). The radial positions of channel residues 431 and 449 are shown in bold. Residue 431 was placed near toxin residue Arg24 and then rotated by 90° about the central axis. Residue 449 was placed 5 Å from the center. The relative positions of 431 and 449 with respect to the subunit borders is arbitrary.

perpendicular to the plane of the membrane.

In contrast, residue 449, which corresponds to the carboxy-terminal limit of the P-region has been shown to be very close to the central axis (Heginbotham and MacKinnon, 1992; Kavanaugh et al., 1992). Therefore, the difference between the radial distance of the amino-terminal end and the carboxy-terminal end of the P-region (see figure 4.5) suggests that the P-region forms a structure where side chains (or backbone carbonyls) from its carboxy-terminal half, rather than the amino terminal half, line the narrow pore and interact with conducting ions. Experiments on ion selectivity are in agreement with this structural proposal. The P-region does not appear to cross the membrane as a hairpin loop, as many transmembrane models propose. The substitution of Asp431 with Asn in the four subunits of the *Shaker* K^+ channel confers toxin insensitivity (table 4.1). However, channels with only a single subunit containing an Asp at position 431 (and the remaining three subunits containing an Asn431) are able to bind toxin with relatively high affinity. This observation could be explained if we consider the interaction between a four-

fold symmetric channel and an asymmetric molecule, the toxin. The toxin can bind to the channel in four energetically equivalent orientations. If only one Asp431 is crucial in a given permissive orientation, then channels with only one Asp431 still have one permissive orientation and, therefore, are sensitive to the toxin. It has been demonstrated that this is the case by studying the interaction between AgTx2 and *Shaker* K^+ channels with different numbers of subunits containing Asp431 (data not shown). The association rate constant for AgTx2 varies with the number of subunits containing Asp431, while the dissociation rate constant remains unchanged. This unique property of the AgTx2-*Shaker* K^+ channel interaction allowed, in the past, deduction of the tetrameric stoichiometry of the channel (MacKinnon, 1991). The present study provides the structural basis underlying this property. Arg24 interacts strongly with Asp431 on only one channel subunit. Asp431 on the diagonal subunit interacts only weakly (with Arg31) and those on the two remaining subunits are located outside the toxin binding site (Figure

4.5). Therefore, as long as the channel contains one Asp431 then the toxin can still bind with high affinity.

Thermodynamic double mutant cycles with a peptide toxin have placed a strong constraint on the structure of the K^+ channel P-region. The extension of this approach to other residues on the toxin and on the channel promises to improve our current picture of the surface structure of the K^+ channel pore.

The method is directly applicable to Na^+, Ca^{2+} and other ion channels where high affinity peptide inhibitors or modulatory proteins are known.

Chapter 5

THERMODYNAMIC COUPLING BETWEEN RESIDUES FORMING THE TOXIN BINDING SITE OF THE *SHAKER* K^+ POTASSIUM CHANNEL SUGGESTS AN α-HELIX FOLDING PATTERN

Two Arg residues, at positions 24 and 31, lying at opposite extremes (25 Å apart) of the AgTx2 structure, were found to interact closely with the same residue on the channel (Asp431, chapter 4 and Hidalgo and MacKinnon, 1995). The four-fold symmetry of the channel together with the toxin's dimensions accounts for these interactions; each Arg residue interacts with Asp431 on a diagonally-opposed channel subunit (figure 5.1). Arg 31 also interacts with Lys427 on the channel as indicated by the Ω analysis (see figure 4.1D and figure 5.2).

A single toxin (Arg31) residue interacting with two different channel residues (K427 and D431) requires a different interpretation; its suggests that those channel

residues are close to each other in space, and, if so they may interact.

For a protein-protein interaction, two amino acid residues in the same polypeptide chain are independent of each other if their individual contributions to binding are additive (Horovitz, 1987). When the residues at positions 427 and 431 of the *Shaker* K^+ channel are both mutated, the magnitude of the equilibrium inhibition constant for toxin inhibition is 30 times lower than expected if residues 427 and 431 were independent.

An extension of the thermodynamic double mutant cycle approach to examine the dependence of a pair-wise toxin-channel interaction on a second channel residue is described in this chapter.

The results from the three way interaction analysis (residues 31 on the toxin and 427 and 431 on the channel) serve to place further constraints on the architecture of the toxin binding site of the *Shaker* K^+ channel.

METHODS

Mutagenesis and expression of AgTx2 and *Shaker* K^+ channel.

Mutagenesis and expression of AgTx2 and the *Shaker* K+ channel were done as described in chapter 4, with the following modification. The double mutant channel K427E-D431N was made by PCR, following the same protocol as for mutation of the toxin (chapter 4, methods section). Two overlapping mutant oligos were synthesized using an Applied Biosystems DNA synthesizer model 391. Two independent PCR reactions with each mutant oligonucleotide were performed. The PCR products were gel purified from a 2% agarose gel and used as primers for a second PCR which covers two restriction sites, Bgl II and BstE II, corresponding to the residues 384 and 437, respectively. The PCR product was phenol extracted, ethanol precipitated, and digested separately with BstE II and then Bgl II. The Bgl II-BstE II fragment was gel purified and ligated to the vector (Bluescript). The mutant clones were confirmed by dideoxy DNA sequencing.

Electrophysiological recording.

The electrophysiological recordings were carried out as described in chapter 4 methods section. The equilibrium inhibition constant (Ki) was calculated according to $Ki = [T](I/I_0)/(1-(I/I_0))$ where I_0 is the control current level and I is the current in the presence of toxin concentration [T].

RESULTS

The coupling coefficient Ω reflects the degree of interaction between two residues brought about by mutation of both residues. Figure 5.1A shows an Ω plot for charge-neutralizing mutations of the eight basic residues on AgTx2 with a channel mutant at position 431 (D431N) (data from figure 4.1). Chapter 4 focused on the description of the coupling between the R24Q/D431N pair and the R31Q/D431N pair and, therefore, on the interaction of two toxin residues (Arg24 and Arg31), which lie on opposite extremes of the toxin, with the same channel residue (Asp431). A detailed analysis of the nature of this interaction together with the known toxin dimensions (chapter 3) and the four-fold symmetry assumed for the K^+ channel give rise to our current picture (figure 5.1B) of the relative orientation of the bound toxin with respect to the channel.

Figure 5.2 shows an Ω plot for the same eight AgTx2 mutants paired with the K427E mutant channel. The Ω value for the R31Q/K427E pair reflects the interaction between

A.

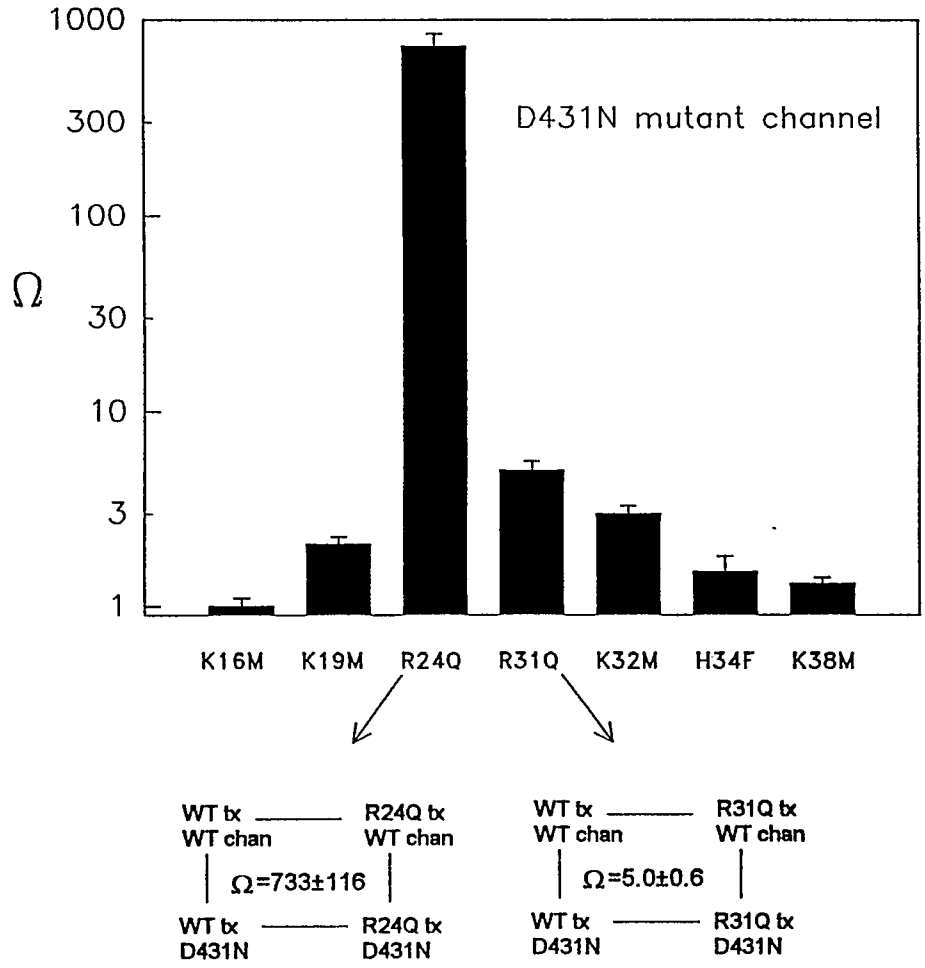

Figure 5.1. (A). Arginines 24 and 31 located on opposite ends of the AgTx2 structure interact with aspartate 431 on diagonally-opposed *Shaker* K^+ channel subunits. **A.** Plot of Ω values for eight AgTx2 charge mutants paired with the D431N channel mutant. The Ω values were calculated according to the following equation (for description see chapter 4); $\Omega = (K_i(wt:wt) \cdot K_i(mut:mut)) / (K_i(wt:mut) \cdot K_i(mut:wt))$, where K_i (toxin:channel) is the equilibrium inhibition constant for the indicated pair, (wt:wt) = wild-type toxin:wild-type channel; (mut:mut) = mutant toxin:mutant channel; (wt:mut) = wild-type toxin:mutant channel and (mut:wt) = mutant toxin:wild-type channel. For easy comparision Ω is reported as a number greater than unity throughout all of these studies. The large Ω value for the R24Q/D431N pair reflects a strong interaction between Arg24 and Asp431. Arg31 also interacts, albeit more weakly, with Asp431 on the opposite channel subunit. The inset corresponds to the double mutant cycle for R24Q/D431N and R31Q/D431N pairs. The equilibrium inhibition constant (Ki) (SEM for 4 to 8 separate measurements) was calculated as described in the methods section.

B.

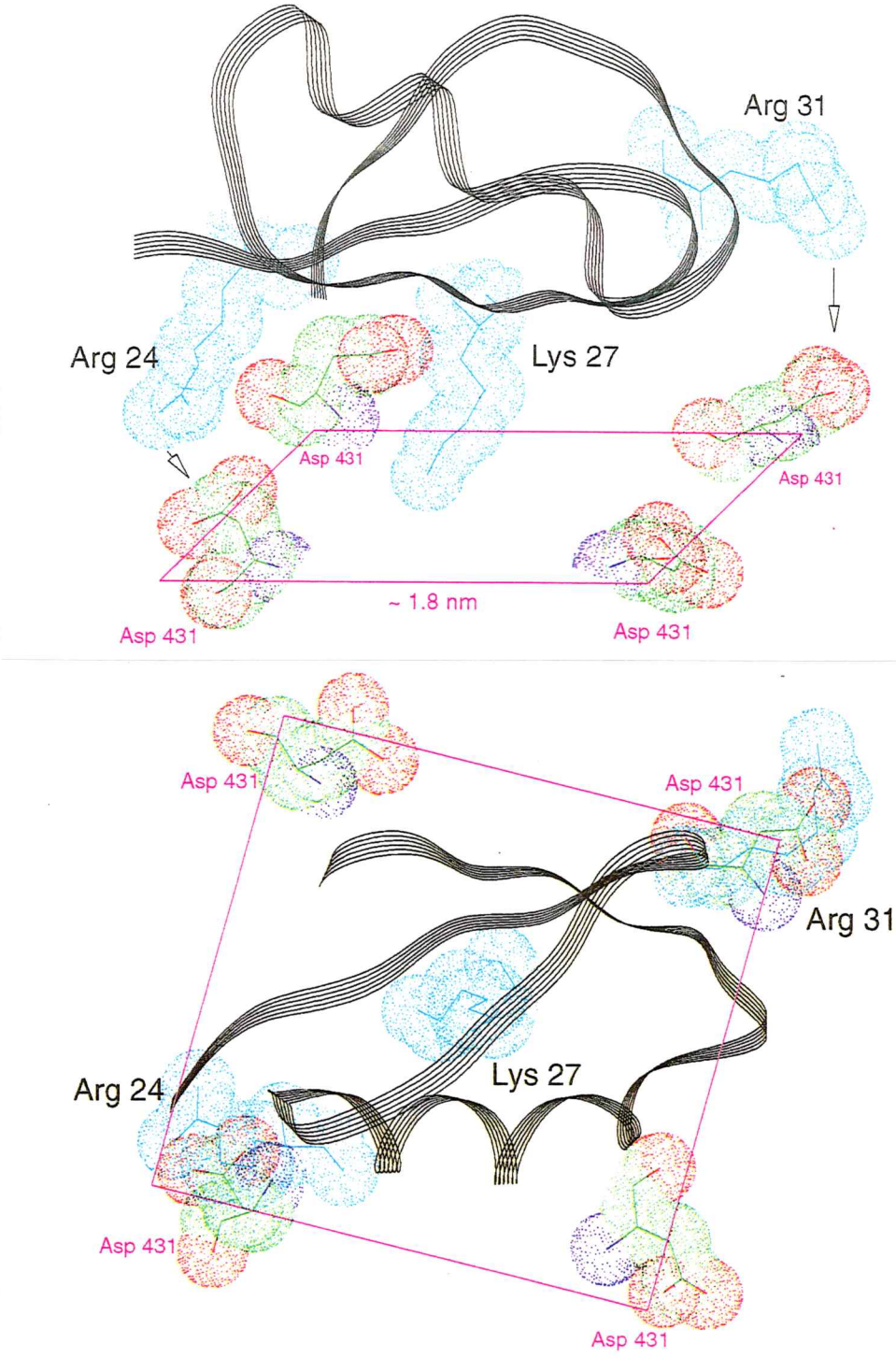

Figure 5.1. (B). Model of AgTx2 bound to the *Shaker* K^+ channel. The backbone of AgTx2 with three side chains, Arg24, Lys27 and Arg31 is shown with their van der Waals surfaces. Lys27 lies over the central axis of the channel (pore). Top panel, lateral view. Bottom panel, top view, 90 rotation of top panel. Arg24 is 25 Å from Arg 31, as are the Asp431 residues located on diagonally-opposed channel subunits (kindly provided by Krezel and MacKinnon).

Arg31 and Lys427. Thus, the same toxin residue, Arg31, interacts with two channel residues, 427 and 431. One toxin residue interacting with two channel residues has a qualitatively different interpretation from the case mentioned above where one channel residue interacts with two toxin residues; it suggests that residues 427 and 431 may lie close to each other, at least when toxin is bound.

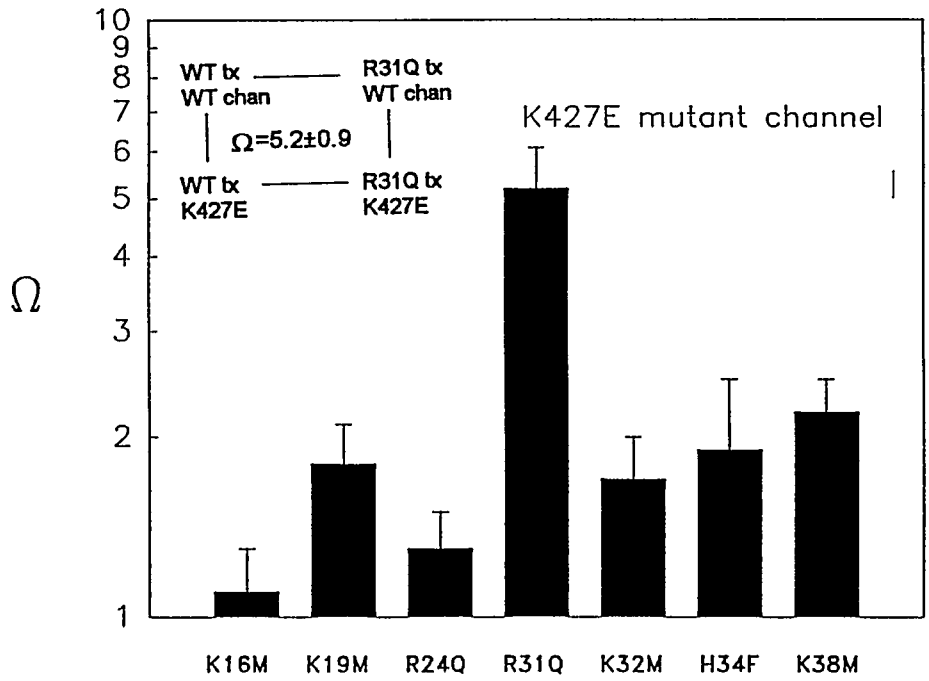

Figure 5.2. Arginine 31 in AgTx2 interacts with residue 427 on the *Shaker* K^+ channel. The plot of Ω values for eight AgTx2 charge mutants paired with the K427E channel mutant is shown. The Ω value for the R31Q/K427E reflects the interaction between Arg31 and Lys427. The inset corresponds to the double mutant cycle for the R31Q/K427E pair. The Ω values were calculated as described in figure 5.1.

To test the nature of the interaction between residues 31 (toxin) and 427 (channel), a network cycle analysis (see also chapter 4 for a complete description) was carried out (figure 5.3). Multiple amino acid substitutions were made at both positions. Two different substitutions at position 31 (Arg with Lys or Gln) paired with three different substitutions at 427 (Lys with Arg, Asn or Glu) give rise to 18 possible cycles. Because the Ω values for the six smallest cycles fully determine Ω values for the remaining cycles, for simplicity, only those cycles are shown. If the coupling in the pair R31Q/K427E comes about by a through-space electrostatic interaction, then perturbing the charge on both residues is the only way to alter the coupling (Ω deviates from unity). All but one of the cycles between the 31/427 pair result in Ω values close to unity. The largest Ω corresponds to a cycle where the charge on both the toxin and the channel were altered (shown in bold). However, another cycle where charge perturbation occurs in both partners (top right) shows an Ω value close to unity. Thus, results from this network cycle analysis of charge alterations at 31 and 427 follow a pattern expected for a

through-space electrostatic interaction when the cycle includes a Glu at 427.

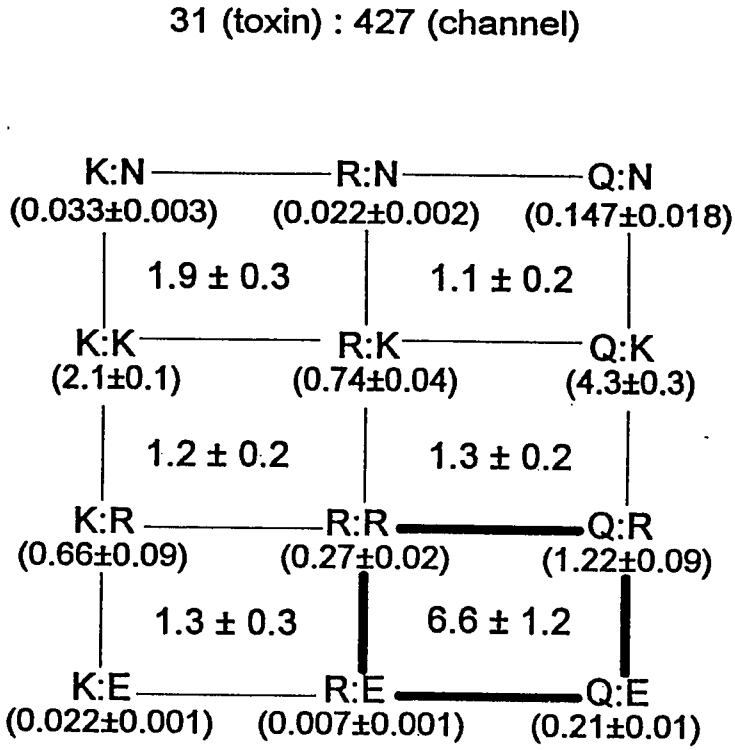

Figure 5.3. Network cycle analysis for the interaction between residue 31 on the toxin and 427 on the channel (see figure 4.3 for complete description of the network cycle analysis). The K_i of AgTx2 for each mutant toxin:channel pair is shown in parentheses at each corner of the cycle (SEM for 4 to 8 separate measurements) and was calculated as described in the methods section.

If channel residue 427 interacts with channel residue 431, that is, if they are not independent, then their individual contributions to the binding of AgTx2 will not be additive. Thus, the binding of the toxin can be used to assess the independence of channel residues 427 and 431. Figure 5.4 shows the thermodynamic double mutant cycle for the K427E/D431N pair. The effect of the channel mutation K427E on AgTx2 affinity was tested in the presence of an Asp at 431 or an Asn at 431 (D431N). The Ω value obtained, approximately 30, reflects an interaction between residue 427 and residue 431, in the context of our toxin blocking assay.

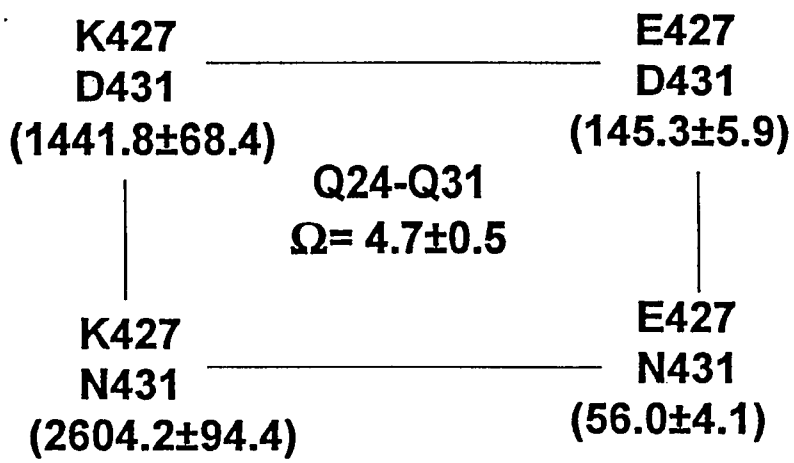

Figure 5.4. Thermodynamic double mutant cycle for the *Shaker* K^+ channel mutant pair K427E/D431N. The Ω value was calculated as in figure 5.1. The K_i of AgTx2 for each pair of channel mutations is shown in parentheses (SEM for 4 to 8 separate measurements).

If residues 427 and 431 are not independent then they must exert a cross influence on their individual interactions with residues 24 and 31 on the toxin. Figure 5.5 shows an Ω plot for the eight charge-neutralizing mutations of AgTx2 paired with K427E (figure 5.5A) and with the D431N channel (figure 5.5B) in the presence or absence of mutations at residue 431 or 427, respectively (table 5.1). The degree of interaction between the R31Q/K427E pair and the R24Q/K427E pair is altered depending on the residue at position 431 (Asp or Asn). The coupling for other mutant toxin-K427E channel pairs are independent of the residue at 431. As expected, the degree of interaction between the R24Q/D431N pair and the R31Q/D431N pair is also influenced by the residue at 427 (Lys or Glu)(figure 5.5b, table 5.1).

A single thermodynamic cycle does not by itself provide information about the interaction between three residues. In others words, no single cycle, such as the ones shown in figures 5.1, 5.2, 5.4 or 5.5, contains information about the dependence of a given pair-wise interaction on a third residue. In order to account for a three-way interaction, a cube describing mutations at the three positions in question must be constructed. Each face

A.

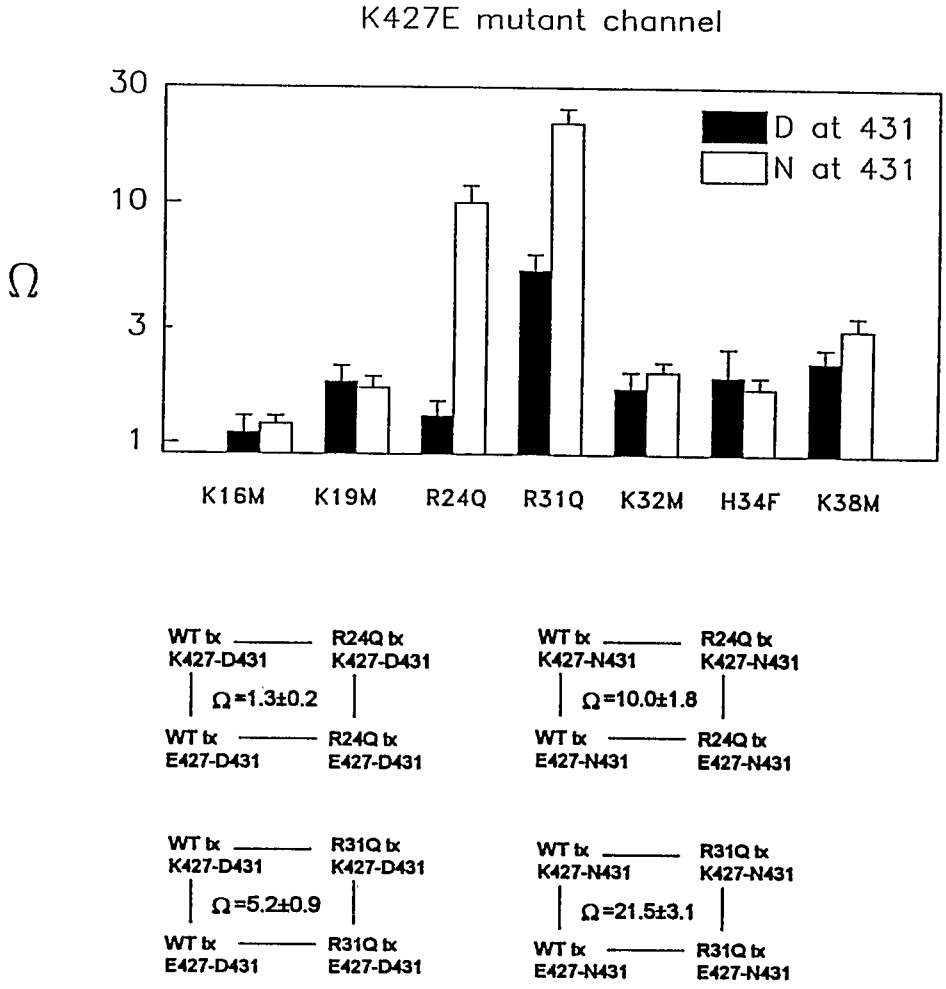

Figure 5.5. (A). Cross influence between *Shaker* K^+ channel residues 427 and 431 on AgTx2 binding. A. Plot of Ω values for eight AgTx2 charge mutants paired with the K427E channel mutant, in the presence of an Asp at 431, black bars (same as figure 5.2), or an Asn at 431, white bars. The inset correspond to the double mutant cycle involving R24Q (top) and R31Q (bottom) in the presence of a D at 431 (left) or an N at 431 (right).

B.

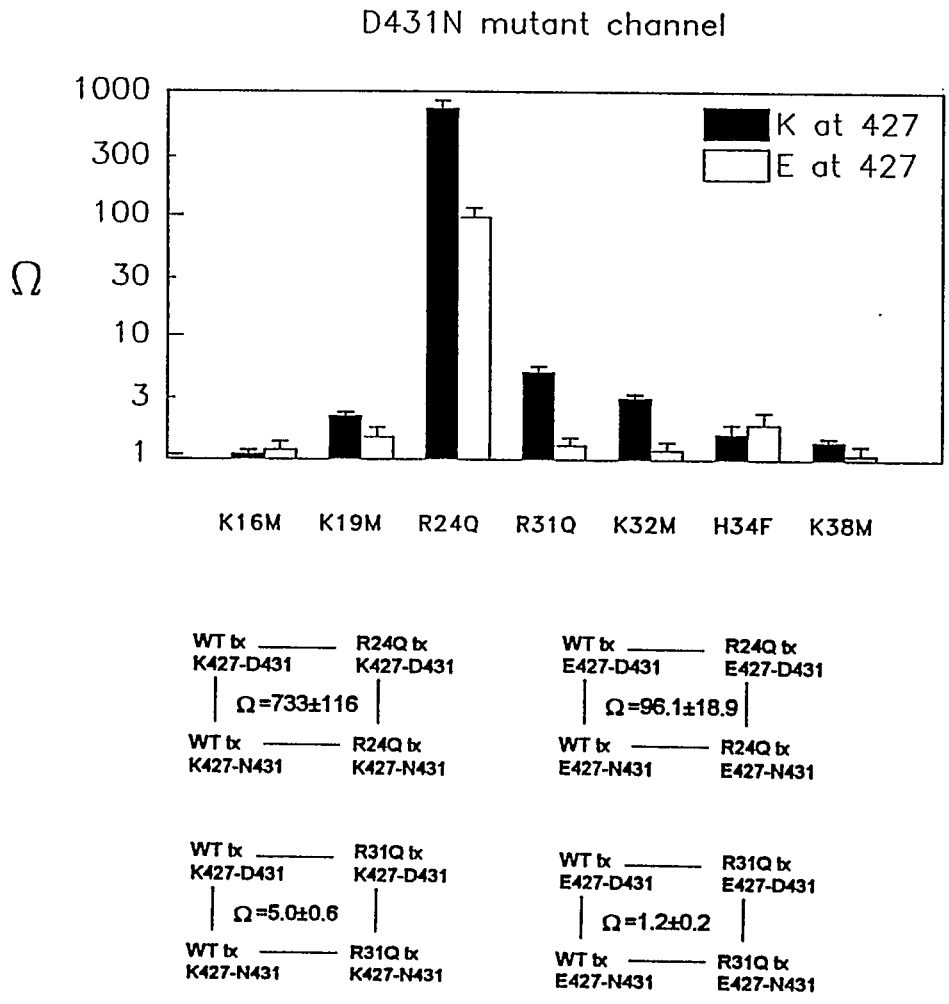

Figure 5.5. B. Plot of Ω values for eight AgTx2 charge mutants paired with the D431N channel mutant, in the presence of a Lys at 427, black bars (same as figure 5.1A), or a Glu at 427, white bars. The inset correspond to the double mutant cycle involving R24Q (top) and R31Q (bottom) in the presence of a K at 427 (left) or an E at 427 (right).

	K16M	K19M	R24Q	R31Q	K32M	H34F	K38M
Ki (nM) K427E-D431N	1.61±0.09	2.0±0.1	9.5±0.8	17.9±1.6	2.9±0.2	0.71±0.07	2.0±0.1
Ω							
K427E (D431)	1.1±0.2	1.8±0.3	1.3±0.2	5.2±0.9	1.7±0.3	1.9±0.6	2.2±0.3
K427E (N431)	1.2±0.1	1.7±0.2	10.0±1.8	21.5±3.1	2.0±0.2	1.7±0.2	3.0±0.4
D431N (K427)	1.0±0.1	2.1±0.2	733±116	5.0±0.6	3.0±0.3	1.5±0.3	1.3±0.1
D431N (E427)	1.1±0.2	1.4±0.3	96.1±18.9	1.2±0.2	1.1±0.2	1.8±0.5	1.0±0.2

Table 5.1. Inhibition constants for the K427E-D431N double mutant channel and Ω values for channel and toxin mutants are tabulated. Each Ki (nM) for the toxin and channel shown was measured as described in methods and is the mean ± SEM of 3 to 8 separate measurements. Ω was calculated as described in figure 5.1. The other Ki values for calculating Ω were taken from table 4.1.

of the cube represents an individual double mutant cycle for a mutated toxin-channel pair or a mutated channel-channel pair. Figure 5.6A shows the cube for the three way interaction observed between the toxin residue 31 and the channel residues 427 and 431. The lateral faces of the cube correspond to the double mutant cycle for the K427E/D431N pair tested with wild-type toxin (right face, figure 5.4) or mutant toxin R31Q (left face). The top and bottom faces correspond to the R31Q/D431N cycle (figure 5.5b), when there is a Lys at 427 (top face) or a Glu (bottom face).

Finally, the front and back faces correspond to the R31Q/K427E cycle (figure 5.5a), when there is an Asp at 431 (front face) or an Asn (back face).

An equivalent cube for the interaction between residues 24 (toxin), 427 and 431 (channel) is shown in figure 5.6B. Notice that the cube involving the mutant toxin at position 24 and the one involving the mutant toxin at position 31 display a common face, corresponding to the double mutant cycle for the K427E/D431N pair tested with wild-type toxin (R24,R31). Figure 5.6C represents the fusion of both cubes, the common face is the lateral one at the center of the double cube. The Ω value for the K427E/D431N pair assayed with wild-type toxin, ($\Omega_{(R,R)}$, central lateral face), decreases if a toxin contains a Gln at position 24, ($\Omega_{(Q,R)}$, right lateral face) or at position 31, ($\Omega_{(R,Q)}$, left lateral face). The product of the Ω values of the external lateral faces equals the value of the central face, i.e. $[\Omega_{(Q,R)} * \Omega_{(R,Q)}] \cong \Omega_{(R,R)}$ (figure 5.6C). Therefore, substitutions of Arg residues at 24 and 31, one at a time, exactly account for the coupling between the K427E/D431N pair, as if the coupling between

K427E/D431N pair comes about exclusively by residues 24 and 31 in the toxin.

When the residues at positions 427 and 431 of the *Shaker* K^+ channel are both mutated (K427E-D431N), the value of the equilibrium inhibition constant (K_i) is 30 times lower than expected if residues 427 and 431 were independent (Table 5.2).

WT	0.74 ± 0.04
K427E	0.007 ± 0.001
D431N	2233 ± 60
K427E-D431N	0.71 ± 0.05

Table 5.2. Inhibition constants for the wild-type channel, the K427E channel, the D431N channel and the double mutant K437E-D431N are shown (SEM for 4 to 8 separate measurements).

The three-way interactions observed between R31, K427 and D431, and analogously between R24, K427 and D431 in the diagonally-opposed channel subunit provide the structural basis for the non-additivity observed for the double mutant channel K427E-D431N (figure 5.5, table 5.2). Residue 24 on the toxin interacts with channel residues 427 and 431 in one subunit, while in the diagonally-opposed channel subunit Arg31 interacts with the same channel residues (figure 5.6D).

A.

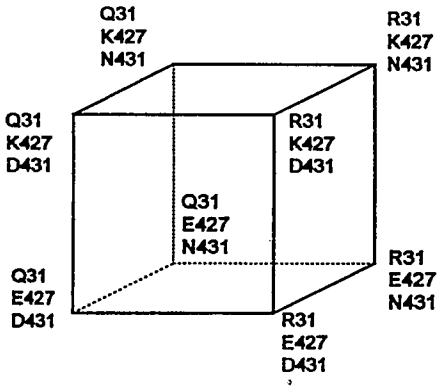
31 (toxin)
Q31
K427
N431
R31
K427
N431
Q31
K427
D431
R31
K427
D431
Q31
E427
N431
R31
E427
N431
Q31
E427
D431
R31
E427
D431

B.

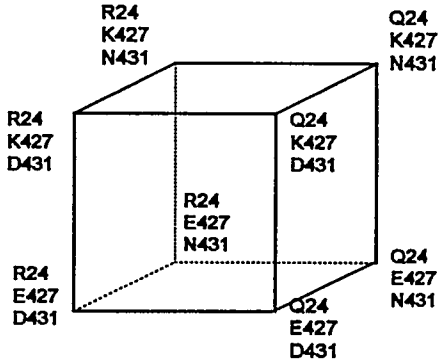
24 (toxin)
R24
K427
N431
Q24
K427
N431
R24
K427
D431
Q24
K427
D431
R24
E427
N431
Q24
E427
N431
R24
E427
D431
Q24
E427
D431

C.

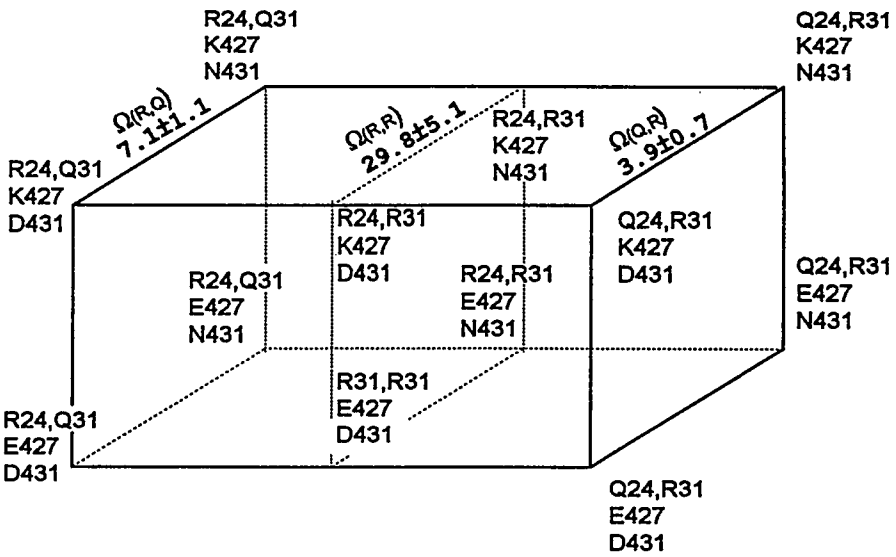
R24,Q31
K427
N431
Q24,R31
K427
N431
Ω(R,Q)
7.1±1.1
Ω(R,R)
29.8±5.1
Ω(Q,R)
3.9±0.7
R24,R31
K427
N431
R24,Q31
K427
D431
R24,R31
K427
D431
Q24,R31
K427
D431
R24,Q31
E427
N431
R24,R31
E427
N431
Q24,R31
E427
N431
R31,R31
E427
D431
R24,Q31
E427
D431
Q24,R31
E427
D431

D.

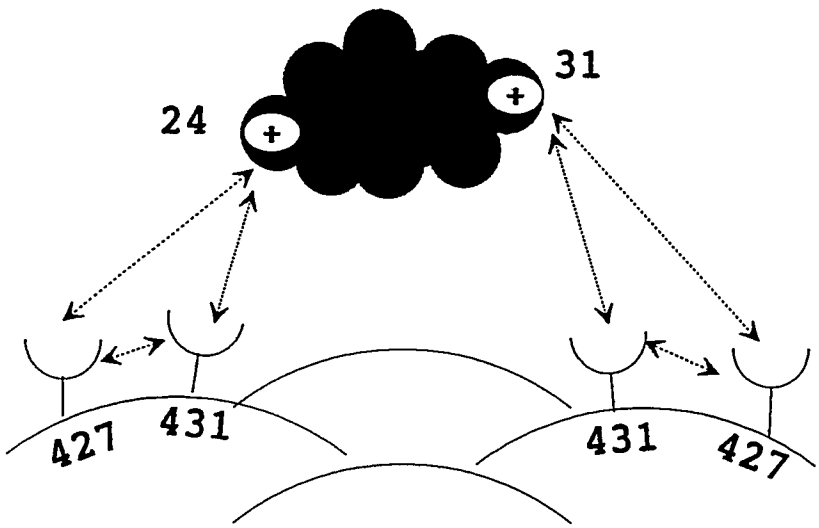
24
31
+
+
427
431
431
427

Figure 5.6. (previous page). A three way interaction is described by a cube of thermodynamic double mutant cycles. For each cube three residues are mutated, one in the toxin, Arg24 (R24Q, left panel) or Arg31 (R31Q, right panel), and two in the channel, Lys427 (K427E) and Asp431 (D431N). Each face of the cube represents an individual double mutant cycle for the given paired mutations. **A.** K427E/D431N channel pair (lateral faces), R31Q/D431N toxin-channel pair (horizontal faces), and R31Q/K427E toxin-channel pair (vertical faces); **B.** K427E/D431N channel pair (lateral faces), R24Q/D431N toxin-channel pair (horizontal faces, and R24Q/K427E toxin-channel pair (vertical faces). **C.** Interaction between three residues in two diagonally-opposed channel subunits are analyzed by two cubes of thermodynamic double mutant cycles. The double cube was constructed by fusion of the cubes shown in panel A. The central double mutant cycle is shared by both cubes shown in panel A and B. **D.** A three way interaction between residues 24 (toxin), 427 and 431 (channel) and between residues 31 (toxin) and 427 and 431 (channel) on the diagonally-opposed channel subunit. AgTx2 is shown in black with Arg24 and Arg31 situated on opposite extremes. Two channel residues, 427 and 431 on diagonally-opposed channel subunits, interact with Arg24 and Arg31. The toxin-channel and channel-channel pair-wise interactions are shown with arrows.

DISCUSSION

The above results demonstrate that channel residues 427 and 431 interact with each other as detected by the toxin inhibition assay. The necessity of placing these two residues close to each other in space constrains the folding pattern formed by this stretch of amino acids on the channel. The results exclude a β-sheet conformation for this segment because the axial distance between adjacent amino acids in a β-sheet structure is approximately 3.5 Å (Creighton, 1993; Branden and Tooze, 1991), which gives a separation of 14 Å between residues 427 and 431. This distance is too large to account for the interaction observed between channel residues 427 and 431. Although our results can not exclude other foldings, for example a β-turn, they are consistent with an α-helix conformation, which could place amino acid residues that are three or four residues apart in the linear sequence spatially close to one another. An α-helix secondary structure would place residues 427 and 431 approximately 6 Å apart (1.5 Å axial distance between adjacent residues, Creighton, 1993;

Branden and Tooze, 1991), and importantly, facing the same side of the helix. In addition, the amino acids between residues 427 and 431, Ser428-Ile429-Pro430, are well conserved among the voltage-activated K^+ channels. Continuing this line of speculation, residue 429 would lie on the opposite face of the helix from 427 and 431, that is to say facing into the plane of the membrane or core of the channel protein. This location would be consistent with its hydrophobic nature.

Preliminary data from Gross and Mackinnon in our laboratory further support an α-helix conformation for a longer stretch of amino acids, which includes the 427 to 431 segment of the S5-S6 linker of the *Shaker* K^+ channel.

In this chapter, an extension of the thermodynamic double mutant cycles approach was used to determine the effect of a third mutation on an interacting toxin-channel pair. The three-way interaction is depicted by a cube of thermodynamic cycles where each face of the cube corresponds to an individual double mutant cycle. Each cycle reflects the energy coupling brought about by the

double mutation between a mutated channel/channel pair or toxin/channel pair.

The results place additional constraints on the architecture of the toxin-binding site in the *Shaker* K^+ channel. They place two channel residues close together in space, implying an α-helix conformation. This is consistent with our previous proposal that part of amino terminal end of the P-region runs parallel rather than perpendicular to the membrane plane (chapter 4).

GENERAL DISCUSSION

K^+ channels are highly specialized enzymes. They are able to discriminate between K^+ and Na^+ ions and allow the flow of K^+ ions from one side of the membrane to the other down their electrochemical gradient. No K^+ channel has yet been purified in large quantities and therefore no conventional structural data are available.

Our current understanding of how K^+ channels operate and the molecular determinants underlying their properties comes from site-directed mutagenesis studies carried out in several laboratories including our own. My thesis work constitutes part of this general effort to understand K^+ channels. I used a scorpion toxin, AgTx2, which binds to the extracellular entryway of the pore, as a structural probe of the *Shaker* K^+ channel. Therefore, the structural data pertain to the most functionally important region of the K^+ channel, the catalytic unit.

In the process of obtaining structural information on a K^+ channel, my work has also contributed to the field of protein-protein interactions. It has provided a new general approach for deducing the spatial organization of amino acids in a linear sequence with respect to a ligand of known structure and has increased our knowledge about protein-protein interaction surfaces.

1. Considerations on the use of AgTx2 as a structural probe of the *Shaker* K^+ channel.

The use of toxin as a caliper for channel dimensions provides information about the receptor in its bound conformation. However, I have reason to believe that the information obtained pertains to the free form of the channel as well. Although little is known about the channel structure, functional data support the idea of minimal conformational change upon binding. First, ChTx can bind to Ca^{2+}-activated K^+ channels in the open and closed states with only a seven-fold lower affinity for the latter (Anderson et al., 1988). If the conformational change resulting from the transition between the open and closed

states still preserves the toxin binding site, this argues that the site is "resistant" to structural changes associated with gating. Second, ChTx bound to the channel is destabilized by permeant ions coming from the cytoplasmic side of the membrane. Impermeant ions do not affect ChTx dissociation (MacKinnon and Miller, 1988). Therefore the selectivity filter of the K^+ channel is not altered by the presence of a bound toxin molecule, making a toxin-induced conformational change unlikely.

2. **Structural integrity of the mutated proteins.**

To draw valid conclusions about structure it is necessary to verify that the mutations in this study do not affect the global conformation of the toxin and the channel. Within the Ω plot there are internal controls for the structural integrity of both proteins. Since most Ω values are close to unity, it is unlikely that the identified coupled interactions arose indirectly through global structural changes.

2.2. AgTx2-*Shaker* K^+ channel interaction

In mapping a protein surface on the basis of pair-wise interactions with a ligand of known structure, a large number of identified contacts should improve the ultimate resolution. Thus, in principle, a system in which many weak interactions contribute to the binding energy gives a higher resolution structural map than one in which a few strong interactions provide most of the energy. AgTx2-*Shaker* K^+ channel interaction appears to be the latter case as suggested by the strong interaction between Arg24 on the toxin and Asp431 on the channel which account for approximately one third of the total binding energy. Clackson and Wells, based on studies of the interaction between the human growth hormone and the extracellular domain of its receptor, had proposed that few amino acid residues contributing to the binding free energy on the protein-protein interface may be a general property of protein-protein contact surfaces. The crystal structure of the complex formed between the human growth hormone and the extracellular domain of its receptor shows that approximately 30 side-chains from each peptide form the

protein-protein interface (de Vos et al., 1992; Clackson and Wells, 1995). However, alanine scanning-mutagenesis of the receptor interaction surface showed that only a few residues on the contact surface are functionally important (Clackson and Wells, 1995). The toxin-channel interaction begins to appear no exception to this emerging pattern for protein-protein interactions in the sense that few contacts may be responsible of the binding affinity.

The specificity of AgTx2 for the *Shaker* K^+ channel may well be based on the ability of Arg24, which is absent in ChTx, to form a hydrogen bond with Asp431.

3. **Relevance of the present work for K^+ channels structure**

The results obtained in my thesis work, summarized in figure 1, constrain the architecture of the pore forming region of the *Shaker* K^+ channel. The amino-terminal residue of the P-region, Asp 431, is placed 12 to 15 Å from the central axis of the K^+ channel (chapter 4 and Hidalgo and MacKinnon, 1995). Therefore, the amino-terminal end of the P-region cannot form the narrow part of the ion conduction pathway. Current transmembrane topology models of K^+

channels depict the P-region as a hairpin that dips symmetrically into the plane of the membrane (figure 1.3). The position assigned to Asp431 by the present work contrasts with these models and suggests that part of the P-region at the amino terminal end runs somewhat parallel to the membrane plane.

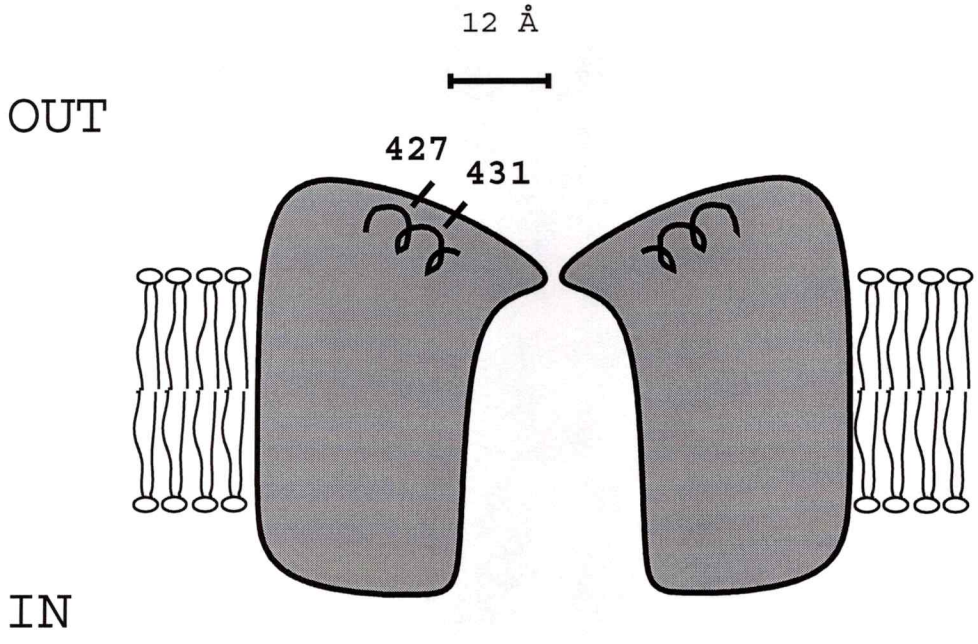

Figure 1. Architecture of the S5-S6 linker of the *Shaker* K^+ channel. The cartoon depicts the structural constrains demonstrated in the present work for the S5-S6 linker of the *Shaker* K^+ channel. The residue Asp 431 is located 12 to 15 Å from the central axis of the K^+ channel. The amino-acid sequence between residues 427 and 431 is proposed to be α-helical.

I have also shown that residues 427 and 431 in the S5-S6 linker are close to each other (chapter 5). Their

physical proximity and the number of amino acids separating them suggest a helical conformation for this segment (figure 1). Thus, the segment of the P-region that runs parallel to the plane of the membrane may adopt a helical conformation, at least over some stretch.

CONCLUSIONS

1.- Recombinat AgTx2 is efficiently expressed in bacteria by recombinant methods and the purified peptide retains its high affinity for the *Shaker* K^+ channel.

2.- AgTx2 accounts for the inhibition of the *Shaker* K^+ channel attributed in previous studies to ChTX.

3.- The solution structure of AgTx2 is similar to that of other K^+ channel inhibitors from scorpion venom. AgTx2 has a triple stranded antiparallel β-sheet, a single helix and three disulfide bonds. Due to its secondary structure and disulfide bridging, AgTx2 is a rigid peptide suitable for using as a caliper to make distance measurement.

4.- The thermodynamic double mutant cycle approach constitutes a systematic method for mapping protein surfaces with a ligand of known structure. This approach

can be immediately applied to other ion channels where high affinity ligands are available.

5.- The amino-terminal end of the P-region of the *Shaker* K^+ channel is situated 12 to 15 Å from the central axis of the channel.

6.- The side chains of residues 427 and 431 in the S5-S6 linker of the *Shaker* K^+ channel are near each other as if the stretch of amino acids between 427 and 431 is α-helical.

BIBLIOGRAPHY

Agus, Z.S., Kelepouris, E., Dukes, I., and Morad, M. (1989). Cytosolic magnesium modulates calcium channel activity in mammalian ventricular cells. *Am. J. Physiol. 256*, C452-C455.

Anderson, C., MacKinnon, R., Smith, C., and Miller, C. (1988). Charybdotoxin inhibition of Ca^{2+}-activated K^+ channels. Effects of channel gating, voltage, and ionic strength. *J. Gen. Physiol. 91*, 317-333.

Anderson, J.A., Huprikar, S.S., Kochian, L.V., Lucas, W.J., and Gaber, R.F. (1992). Functional expression of a probable *Arabidopsis thaliana* potassium channel in *Saccharomyces cervisiae*. *Proc. Natl. Acad. Sci. USA 89*, 3736-3740.

Atkinson, N.S., Robertson, G.A., and Ganetzky, B. (1991). A component of calcium-activated potassium channels encoded by the *Drosophila slo* locus. *Science 253*, 551-555.

Baumann, A., Grupe, A., Ackermann, A., and Pongs, O. (1988). Structure of the voltage-dependent potassium channel is highly conserved from *Drosophila* to vertebrate central nervous systems. *EMBO J. 7*, 2457-2463.

Bontems, F., Gilquin, B., Roumestand, C., Menez, A., and Toma, F. (1992). Analysis of side-chain organization on a refined model of Charybdotoxin: structural and functional implications. *Biochemistry 31*, 7756-7764.

Bontems, F., Roumestand, C., Gilquin, B., Menez, A., and Toma, F. (1991a). Refined structure of Charybdotoxin: common motifs in scorpion toxins and insect defensins. *Science 254*, 1521-1523.

Bontems, F., Roumestand, C., Boyot, P., Gilquin, B., Doljansky, Y., Menez, A., and Toma, F. (1991b). Three-dimensional structure of natural Charybdotoxin in aqueous solution by ^{1}H-NMR. *Eur. J. Biochem. 196*, 19-28.

Branden, C. and Tooze, J. (1991). Introduction to protein structure (New York: Garland Publishing, Inc.).

Bruggemann, A., Pardo, L.A., Stühmer, W., and Pongs, O. (1993). Ether-a-go-go encodes a voltage-gated channel permeable to K^+ and Ca^{2+} and modulated by cAMP.. *Nature (London) 365*, 445-448.

Butler, A., Wei, A., Baker, K., and Salkoff, L. (1989). A family of putative potassium channel genes in *Drosophila*. *Science 243*, 943-947.

Butler, A., Tsunoda, S., McCobb, D.P., Wei, A., and Salkoff, L. (1993). m*Slo*, a complex mouse gene encoding "Maxi" calcium-activated potassium channels. *Science 261*, 221-224.

Candia, S., García, M.L., and Latorre, R. (1992). Mode of action of Iberiotoxin, a potent blocker of the large conductancer Ca^{2+}-activated K^+ channel. *Biophys. J. 63*, 583-590.

Carter, P.J., Winter, G., Wilkison, A.J., and Fersht, A.R. (1984). The use of double mutants to detect structural changes in the active site of the tyrosyl-tRNA synthetase (*Bacillus stearothermophilus*). *Cell 38*, 835-840.

Catterall, W.A. (1988). Structure and function of voltage-sensitive ion channels. *Science 242*, 50-61.

Choi, K.L., Mossman, C., Aube, J., and Yellen, G. (1993). The internal quaternary ammonium receptor site of *Shaker* potassium channels. *Neuron 10*, 533-541.

Clackson, T. and Wells, J.A. (1995). A hot spot of binding energy in a hormone-receptor interface. *Science 267*, 383-386

Creighton, T. E. (1993). Proteins: structure and molecular properties (New York: second edition. W.H. Freeman Company)

De Biasi, M., Kirsch, G.E., Drewe, J.A., Hartmann, H.A., and Brown, A.M. (1993). Cesium selectivity conferred by histidine substitution in the pore of the potassium channel Kv2.1. *Biophys. J. 64*, A341

De Vos, A.M., Ultsch, M., and Kossiakoff, A.A. (1995). Human growth hormone and extracellular domain of its receptor: crystal structure of the complex. *Science 255*, 306-312.

Fernandez, I., Romi, R., Szendeffy, S., Martin-Eauclaire, M.F., Rochat, H., van Rietschoten, J., Pons, M., and Giralt, E. (1994). Kaliotoxin (1-37) shows structural differences with related potassium channel blockers. *Biochemistry 33*, 14256-14263.

Frech, G.C., VanDongen, A.M.J., Schuster, G., Brown, A.M., and Joho, R.H. (1989). A novel potassium channel with delayed rectifier properties isolated from rat brain by expression cloning. *Nature (London) 340*, 642-645.

Gálvez, A., Gimenez-Gallego, G., Reuben, J.P., Roy-Contancin, L., Feigenbaum, P., Kaczorowski, G.J., and García, M.L. (1990). Purification and characterization of a unique, potent, peptidyl probe for the high conductance calcium-activated potassium channel from venom of the scorpion *Buthus tamulus*. *J. Biol. Chem. 265*, 11083-11090.

García, M.L., García-Calvo, M., Hidalgo, P., Lee, A., and MacKinnon, R. (1994). Purification and characterization of three inhibitors of voltage-dependent K^+ channels from *Leiurus quinquestriatus* var. *hebraeus* venom. *Biochemistry 33*, 6834-6839.

García, M.L., Gálvez, A., García-Calvo, M., King, V.F., Vazquez, J., and Kaczorowski, G.J. (1991). Use of toxins to study potassium channels. *Journal of Bioenergetics and Biomembranes 23*, 615-646.

García-Calvo, M., Leonard, R.J., Novick, J., Stevens, S.P., Schmalhofer, W., Kaczorowski, G.J., and García, M.L. (1993). Purification, characterization and biosynthesis of Margatoxin, a component of *Centuroides margaritatus* venom that selectively inhibits voltage-dependent potassium channels. *J. Biol. Chem. 268*, 18866-18874.

Giangiacomo, K.M., García, M.L., and McManus, O.B. (1992). Mechanism of Iberiotoxin block of the large conductance calcium-activated potassium channel from bovine aortic smooth muscle. *Biochemistry 31*, 6719-6727.

Gimenez-Gallego, G., Navia, M.A., Reuben, J.P., Katz, G.M., Kaczorowski, G.J. and García, M.L. (1988). Purification, sequence, and model structure of Charybdotoxin, a potent selective inhibitor of calcium activated potassium channels. *Proc. Natl. Acad. Sci. USA 85*, 3329-3333.

Goldstein, S. and Miller, C. (1993). Mechanism of Charybdotoxin block of a voltage-gated K^+ channel. *Biophys. J. 65*, 1613-1619.

Goldstein, S., Pheasant, D.J., and Miller, C. (1994). The Charybdotoxin receptor of a *Shaker* K^+ channel: peptide and channel residues mediating molecular recognition. *Neuron 12*, 1377-1388.

Gross, A., Abramson, T., and MacKinnon, R. (1994). Transfer of the scorpion toxin receptor to an insensitive potassium channel. *Neuron 13*, 961-966.

Hartmann, H.A., Kirsch, G.E., Drewe, J.A., Taglialatela, M., Joho, R.H., and Brown, A.M. (1991). Exchange of conduction pathways between two related K^+ channels. *Science 251*, 942-944.

Heginbotham, L. and MacKinnon, R. (1992). The aromatic binding site for tetraethylammonium ion on potassium channels. *Neuron 8*, 483-491.

Heginbotham, L., Abramson, T., and MacKinnon, R. (1992). A functional connection between the pores of distantly related ion channel as revealed by mutant K^+ channels. *Science 258*, 1152-1155.

Heginbotham, L., Lu, Z., Abramson, T., and MacKinnon, R. (1994). Mutations in the K^+ channel signature sequence. *Biophys. J. 66*, 1061-1067.

Hidalgo, P. and MacKinnon, R. (1995). Revealing the architecture of a K^+ channel pore through mutant cycles with a peptide inhibitor. *Science 268*, 307-310.

Hille, B. (1973). Potassium channels in myelinated nerve. Selective permeability to small cations. *J. Gen. Physiol. 61*, 669-686.

Hille, B. (1975). Ionic selectivity of Na and K channels of nerve membranes (New York: Marcel Dekker).

Ho, K., Nichols, C.G., Lederer, W.J., Lytton, J., Vassilev, P.M., Kanazirska, M.V., and Hebert, S.C. (1993). Cloning and expression of an inwardly rectifying ATP-regulated potassium channel. *Nature (London) 362*, 31-38.

Horovitz, A. (1987). Non-additivity in protein-protein interactions. *J. Mol. Biol. 196*, 733-735.

Horovitz, A. and Fersht, A.R. (1990). Strategy for analysing the co-operativity of intramolecuar interactions in peptides and proteins. *J. Mol. Biol. 214*, 613-617.

Hoshi, T., Zagotta, W.N., and Aldrich, R.W. (1990). Biophysical and molecular mechanisms of *Shaker* potassium channel inactivation. *Science 250*, 533-538.

Jan, L.Y. and Jan, Y.N. (1990). A superfamily of ion channels. *Nature (London) 345*, 672

Jan, L.Y. and Jan, Y.N. (1994). Potassium channels and their evolving gates. *Nature 371*, 119-122.

Johnson, B.A. and Snugg, E.E. (1992). Determination of the three dimensional structure of Iberiotoxin in solution by ^{1}H nuclear magnetic resonance spectroscopy. *Biochemistry 31*, 8151-8159.

Johnson, B.A., Stevens, S.P., and Williamson, J.M. (1994). Determination of the three-dimensional structure of Margatoxin by ^{1}H, ^{13}C, ^{15}N triple-resonance nuclear magnetic resonance spectroscopy. *Biochemistry 33*, 15061-15070.

Kamb, A., Tseng-Crank, J., and Tanouye, M.A. (1988). Multiple products of the *Drosophila Shaker* gene may contribute to potassium channel diversity. *Neuron 1*, 421-430.

Kavanaugh, M.P., Hurst, R.S., Yakel, J., Varnum, M.D., Adelman, J.P., and North, R.A. (1992). Multiple subunits of a voltage-dependent potassium channel contribute to the binding site for tetraethylammonium. *Neuron 8*, 493-497.

Kavanaugh, M.P., Varnum, M.D., Osborne, P.B., Christie, M.J., Busch, A.E., Adelman, J.P., and North, R.A. (1991). Interaction between tetraethylammonium and amino acid residues in the pore of cloned voltage-dependent potassium channels. *J. Biol. Chem. 266*, 7583-7587.

Kirsch, G.E., Drewe, J.A., Hartmann, H.A., Taglialatela, M., de Biasi, J., Brown, A.M., and Joho, R.H. (1992). Differences between the deep pores of K^{+} channels determined by an interacting pair of nonpolar amino acids. *Neuron 8*, 499-505.

Krezel, A., Khasibhatla, C., Hidalgo, P., MacKinnon, R., and Wagner, G. (1995). Solution structure of the potassium channel inhibitor Agitoxin 2: Calipers for probing channel geometry. *Prot. Sci. In Press*,

Kubo, Y., Baldwin, T.J., Yan, Y.N., and Jan, L.Y. (1993a). Primary structure and functional expression of a mouse inward rectifier potassium channel. *Nature (London) 362*, 127-132.

Kubo, Y., Reuveny, E., Slesinger, P.A., Jan, Y.N., and Jan, L.Y. (1993b). Primary structure and functional expression of a rat G-protein-coupled muscarinic potassium channel. *Nature (London) 364*, 802-806.

Kunkel, T.A. (1985). Rapid and efficient site-specific mutagenesis without phenotypic selection. *Proc. Natl. Acad. Sci. U. S. A. 82*, 488-492.

López, G.A., Jan, Y.N., and Jan, L.Y. (1994). Evidence that the S6 segment of the *Shaker* voltage-gated K^+ channel comprises part of the pore. *Nature 367*, 179-182.

Lucchesi, K., Ravindran, A., Young, H., and Moczydlowski, E. (1989). Analysis fo the blocking activity of Charybdotoxin homologs and iodinated derivatives against Ca^{2+}-activated K^+ channels. *J. Membr. Biol. 109*, 269-281.

MacKinnon, R. (1991). Determination of the subunit stoichiometry of a voltage-activated potassium channel. *Nature (London) 350*, 232-235.

MacKinnon, R. and Miller, C. (1988). Mechanism of charybdotoxin block of Ca^{2+}-activated K^+ channels. *J. Gen. Physiol. 91*, 335-349.

MacKinnon, R. and Miller, C. (1989a). Mutant potassium channels with altered binding of Charybdotoxin, a pore-blocking peptide inhibitor. *Science 245*, 1382-1385.

MacKinnon, R. and Miller, C. (1989b). Functional modification of a Ca^{2+}-activated K^+ channel by trimethyloxonium. *Biochemistry 28*, 8087-8092.

MacKinnon, R. and Yellen, G. (1990). Mutations affecting TEA blockade and ion permeation in voltage-activated K^+ channels. *Science 250*, 276-279.

MacKinnon, R., Heginbotham, L., and Abramson, T. (1990). Mapping the receptor site for Charybdotoxin, a pore-blocking potassium channel inhibitor. *Neuron 5*, 767-771.

MacKinnon, R., Latorre, R., and Miller, C. (1989). Role of surface electrostatics in the operation of a high-conductance Ca^{2+}-activated K^+ channel. *Biochemistry 28*, 8092-8099.

MacKinnon, R., Reinhart, P.H., and White, M.M. (1988). Charybdotoxin block of *Shaker* K^+ channels suggests that

different types of K^+ channels share common structural features. *Neuron 1*, 997-1001.

Miller, C., Moczydlowski, E., Latorre, R., and Phillips, M. (1985). Charybdotoxin, a high-affinity inhibitor of single Ca^{2+}-activated K^+ channels of mammalian skeletal muscle. *Nature (London) 313*, 316-318.

Oliva, C., Folander, K., and Smith, J.S. (1991). Charybdotoxin is not a high affinity blocker of *Shaker* K^+ channels expressed in *Xenopus* oocytes. *Biophys. J. 59*, 450A.

Pak, M.D., Baker, K., Covarrubias, M., Butler, A., Ratcliffe, A., and Salkoff, L. (1991). mShal, a subfamily of A-type K^+ channel cloned from mammalian brain. *Proc. Natl. Acad. Sci. USA 88*, 4386-4390.

Park, C.S. and Miller, C. (1992a). Interaction of Charybdotoxin with permeant ions inside the pore of a K^+ channel. *Neuron 9*, 307-313.

Park, C.S. and Miller, C. (1992b). Mapping function to structure in a channel-blocking peptide: electrostatic mutants of charybdotoxin. *Biochemistry 31*, 7749-7755.

Park, C.S., Hausdorff, S.F., and Miller, C. (1990). Design, synthesis, and functional expression of a gene for Charybdotoxin, a peptide blocker of K^+ channels. *Proc. Natl. Acad. Sci. U. S. A.*

Pongs, O., Kecskemethy, N., Müller, R., Krah-Jentgens, I., Baumann, A., Kiltz, H.H., Canal, I., Llamazares, S., and Ferrus, A. (1988). *Shaker* encodes a family of putative potassium channel proteins in the nervous system of *Drosophila*. *EMBO J. 7*, 1087-1096.

Possani, L.D., Martin, B.M., and Svendsen, I.B. (1982). *Carlsberg Res. Commun. 47*, 285-289.

Romi, R., Crest, M., Gola, M., Sampieri, F., Jacquet, G., Zerrouk, H., Mansuelle, P., Sorokine, O., van Dorsselaer, A., Rochat, H., Martin-Eauclaire, M.F., and Van Rietschoten, J. (1993). Synthesis and characterization of Kaliotoxin. *J. Biol. Chem. 268*, 26302-26309.

Sanger, F., Nicklen, S., and Coulson, A.R. (1977). DNA sequencing with chain-terminating inhibitors. *Proc. Natl. Acad. Sci. U. S. A. 74*, 5463-5467.

Schachtman, D.P., Schroeder, J.I., Lucas, W.J., Anderson, J.A., and Gaber, R.F. (1992). Expression of an inward-rectifying potassium channel by the *Arabidopsis* KAT1 cDNA. *Science 258*, 1654-1658.

Sentenac, H., Bonneaud, N., Minet, M., Lacroute, F., Salmon, J.M., Gaymard, F., and Gignon, C. (1992). Cloning and expression in yeast of a plant potassium ion transport system. *Science 256*, 663-665.

Serrano, L., Horovitz, A., Avron, B., Bycroft, M., and Fersht, A.R. (1990). Estimating the contribution of engineered surface electrostatic interactions to protein stability by using double-mutant cycles. *Biochemistry 29*, 9343-9352.

Slesinger, P.A., Jan, Y.N., and Jan, L.Y. (1993). The S4-S5 loop contributes to the ion-selective pore of potassium channels. *Neuron 11*, 739-749.

Stampe, P., Kolmakova-Partensky, L., and Miller, C. (1994). Intimations of K^+ channel structure from a complete functional map of the molecular surface of Charybdotoxin. *Biochemistry 33*, 443-450.

Tempel, B.L., Papazian, D.M., Schwarz, T.L., Jan, Y.N., and Jan, L.Y. (1987). Sequence of a probable potassium channel component encoded at *Shaker* locus of *Drosophila*. *Science 237*, 770-775.

Timpe, L.C., Schwarz, T.L., Tempel, B.L., Papazian, D.M., Jan, Y.N., and Jan, L.Y. (1988). Expression of functional potassium channels from *Shaker* cDNA in *Xenopus* oocytes. *Nature (London) 331*, 143-145.

Warmke, J., Drysdale, R., and Ganetzky, B. (1991). A distinct potassium channel polypeptide encoded by the *Drosophila eag* locus. *Science 252*, 1560-1562.

Wei, A., Covarrubias, M., Butler, A., Baker, K., Pak, M., and Salkoff, L. (1990). K^+ channel diversity is produced by an extended gene family conserved in *Drosophila* and mouse. *Science 248*, 599-603.

Yellen, G., Jurman, M., Abramson, T., and MacKinnon, R. (1991). Mutations affecting internal TEA blockade identify the probable pore-forming region of a K^+ channel. *Science 251*, 939-941.

Yokoyama, S., Imoto, K., Kawamura, T., Higashida, H., Iwabe, N., Miyata, T., and Numa, S. (1989). Potassium

channels from NG108-15 neuroblastoma-glioma hybrid cells: Primary structure and functional expression from cDNAs. *FEBS Lett. 259*, 37-42.

Yool, A.J. and Schwarz, T.L. (1991). Alteration of ionic selectivity of a K^+ channel by mutation of the H5 region. *Nature (London) 349*, 700-704.